land

Article

Unmasking Non-Static Drivers of Urban Ecological Resilience: Evidence from the Guanzhong Plain Urban Agglomeration

Xiaohui Ding [1,*], Yuan Wang [1], Kehui Li [1], Ruolan Li [1] and Heng Wang [2]

[1] Northwest Institute of Historical Environment and Socio-Economic Development, Shaanxi Normal University, Xi'an 710119, China
[2] School of Economics and Management, Xianyang Normal University, Xianyang 712000, China
* Correspondence: xhding@snnu.edu.cn

Abstract

Urban ecological resilience (UER) has become a central concern in rapidly urbanizing regions where development pressures increasingly interact with ecological constraints. Focusing on the Guanzhong Plain Urban Agglomeration (GPUA), a semi-arid urban agglomeration in western China, this study examines the non-static and locally heterogeneous drivers of UER across 11 prefecture-level cities from 2000 to 2023. UER is measured through resistance, adaptability, and recovery. An extended STIRPAT model, Elastic Net with stability selection, two-way fixed-effects period interactions, and Geographically and Temporally Weighted Regression (GTWR) are integrated to identify robust drivers, test post-2011 shifts, and estimate city-year local associations. Residual Moran's I diagnostics and Spatial Lag GTWR (SLM-GTWR) are used as supplementary checks. The results show that UER remains relatively stable at the aggregate regional level but becomes increasingly divergent across cities. Ten robust drivers are retained, with fiscal investment intensity, human capital, medical and health level, and total energy consumption emerging as key variables. Period heterogeneity results indicate that fiscal investment becomes more favorably associated with UER after 2011, while the marginal association of energy consumption weakens. GTWR reveals clear local heterogeneity: human capital shows the most stable positive association, medical and health level remains generally negative, fiscal investment is positive but context-dependent, and energy consumption is predominantly negative but locally differentiated. Supplementary spatial diagnostics suggest that the GTWR specification captures the main spatiotemporal structure of UER, while spatial-lag checks broadly support the robustness of the local coefficient patterns, although estimates of spatial interaction remain sensitive to how inter-city linkages are defined. These findings indicate that UER drivers are dynamic rather than fixed, with resilience formation shaped mainly by governance-regime shifts and localized heterogeneity. The study contributes a sequential screening–heterogeneity framework for identifying non-static resilience drivers and suggests that resilience governance should combine stage-sensitive policy adjustment, place-based intervention, and regional coordination where ecological functions and environmental risks cross administrative boundaries.

Keywords: urban ecological resilience; spatiotemporal heterogeneity; spatial diagnostics; STIRPAT; GTWR

Check for updates

Academic Editor: Shiliang Liu

Received: 17 May 2026
Revised: 29 June 2026
Accepted: 29 June 2026
Published: 3 July 2026

1. Introduction

Urbanization is increasingly unfolding under binding ecological constraints. As the principal loci of anthropogenic activity, cities occupy less than 3% of the Earth's land surface yet account for over 70% of global carbon emissions and resource consumption, making them central spaces of ecological vulnerability in the Anthropocene [1,2]. Consequently, urban ecological resilience (UER)—the capacity of urban socio-ecological systems to absorb disturbances, reorganize, and sustain functionality under stress—has become a key concern in sustainable urban planning and governance [3]. This challenge is especially acute in China, where rapid urbanization over the past four decades has generated severe environmental degradation [4]. In response, the national development agenda has shifted from a "speed-first" model toward "high-quality development" and "Ecological Civilization," as reflected in the 12th Five-Year Plan (2011–2015) and subsequent policy frameworks [5].

The Guanzhong Plain Urban Agglomeration (GPUA) provides a representative setting for examining resilience formation under such constraints. Located in the ecologically fragile Yellow River Basin of western China, the GPUA is a typical semi-arid urban agglomeration facing the dual pressures of water scarcity and rapid industrialization. As a strategic node of the "Belt and Road Initiative," its development trajectory reflects the tension between urban expansion and ecological conservation, particularly in relation to the Qinling Mountains—often referred to as China's "central national park" [6]. Unlike coastal megalopolises with relatively stronger environmental carrying capacity, the GPUA must navigate a narrower corridor between growth and ecological protection. Understanding resilience dynamics in this region therefore offers broader insights for emerging economies attempting to reconcile development with ecological security.

To support such governance challenges, policymakers need evidence on how socioeconomic factors are associated with resilience outcomes. The STIRPAT (Stochastic Impacts by Regression on Population, Affluence, and Technology) framework has been widely used for this purpose [7]. However, existing STIRPAT-based resilience studies still lack a coherent framework for understanding resilience drivers as dynamic and context-dependent relationships. The existing literature has largely examined whether socioeconomic or environmental factors are associated with resilience outcomes, while paying less attention to whether their meanings, elasticities, and governance implications change across development stages and local contexts. In this study, this broader gap is understood as the problem of non-static drivers: resilience determinants should not be treated as fixed and universal elasticities, but as relationships that may vary across policy regimes, ecological constraints, and place-specific development pathways. This gap is reflected in three related aspects.

First, the identification of resilience drivers remains unstable under high-dimensional and correlated indicator systems. Urban resilience is influenced by multiple interrelated factors, yet conventional econometric models perform poorly when predictors are numerous and highly correlated. Many studies continue to rely on ad hoc variable selection based on the prior literature or stepwise regression procedures [8,9]. Such practices may retain spurious predictors while omitting substantively important ones because of multicollinearity between affluence- and technology-related proxies, thereby weakening both coefficient stability and interpretability [10]. This statistical instability also has substantive implications: it obscures which mechanisms should be examined for temporal and spatial non-staticity.

Second, existing studies rarely explain how driver elasticities and policy meanings change across development stages. Many STIRPAT applications still impose temporally fixed coefficients, obscuring structural changes around major policy turning points and governance transitions. Yet the same driver may have different implications under different policy regimes. For example, fiscal investment may be more closely related to land development and infrastructure expansion in an expansion-oriented stage, but may become more connected with ecological restoration, environmental infrastructure, and governance capacity under a sustainability-oriented regime. Similarly, energy consumption may reflect ecological pressure differently depending on energy efficiency improvement, industrial upgrading, and environmental regulation. Therefore, a regime-sensitive framework is needed not only to detect coefficient changes, but also to interpret how policy transitions reshape the mechanisms through which drivers are associated with UER.

Third, the place-specific nature of resilience drivers remains insufficiently theorized and diagnosed. Urban agglomerations contain cities with different ecological endowments, industrial structures, fiscal capacities, human capital bases, and environmental pressures. As a result, the same driver may show different local associations across cities. While Geographically Weighted Regression (GWR) and Geographically and Temporally Weighted Regression (GTWR) can capture local heterogeneity [11,12], spatial analysis in small regional samples should not assume spillovers as a dominant mechanism a priori, because spatial dependence estimates are sensitive to the definition of spatial weights. A more cautious approach is therefore needed: local heterogeneity should first be identified through GTWR, residual spatial dependence should then be diagnosed using alternative spatial weights matrices, and spatial-lag models should be used as supplementary robustness checks rather than as the primary basis for claiming strong spatial spillovers.

To address these gaps, this study develops an integrated framework that combines machine-learning-based variable screening, structural-break analysis, GTWR-based local heterogeneity modeling, and residual spatial dependence diagnostics. First, Elastic Net regularization with stability selection is used to screen a broad set of urban sustainability indicators in a systematic and reproducible manner [13]. This step mitigates multicollinearity and noise, yielding a parsimonious subset of robust drivers. Second, building on the STIRPAT framework, a two-way fixed-effects specification with time-varying interactions is employed to test for structural shifts around the pivotal year 2011 [5]. This "screening-then-heterogeneity" design makes it possible to identify policy-induced changes in elasticity that static models would conceal. Third, GTWR is used to estimate continuous city–year local coefficients and reveal the spatially heterogeneous and temporally evolving associations between UER and key drivers. Residual spatial dependence is evaluated using baseline ($k = 3$) and alternative spatial weights. SLM-GTWR serves as a supplementary robustness check to verify the stability of GTWR patterns after introducing a spatial-lag term, rather than as the primary basis for claiming strong spatial spillovers.

Furthermore, recent research recognizes that the influence of drivers is not temporally or spatially invariant. Adaptive resilience theory and evolutionary urban system perspectives [3,14–16] regard resilience formation as a dynamic process in which driver effectiveness evolves across development stages and geographical contexts. As urban systems transition from expansion-oriented growth to sustainability-oriented governance, the marginal effects of fiscal investment, human capital, energy consumption, and public services may change substantially across policy regimes and governance contexts. Likewise, cities with different economic structures, resource endowments, and governance capacities may exhibit heterogeneous responses to identical drivers [2]. Consequently, resilience drivers should not be conceptualized as fixed elasticities but rather as dynamic relationships conditioned by temporal evolution and spatial context. This perspective motivates the present study's focus on identifying the non-static drivers of urban ecological resilience.

Overall, this study contributes to the literature by advancing a non-static understanding of urban ecological resilience drivers. The central contribution is not simply the use of multiple empirical techniques, but the construction of a sequential framework for explaining how resilience–driver associations vary across policy stages and local contexts. Its contribution is threefold. First, at the conceptual level, the study reframes resilience drivers as dynamic and context-dependent relationships rather than fixed elasticities. By linking adaptive resilience theory with evolutionary urban systems perspectives, it emphasizes that the same socioeconomic driver may have different meanings under different governance regimes and local ecological conditions. Second, at the methodological level, the study develops a screening–heterogeneity analytical strategy. Elastic Net with stability selection is used to identify a reproducible set of robust drivers from a high-dimensional and collinear candidate pool. TWFE period-interaction models then examine whether these driver–UER associations shift after the 2011 policy transition. GTWR further reveals city–year local heterogeneity, while residual spatial diagnostics and supplementary SLM-GTWR checks are used to assess the stability of the spatial interpretation without treating spillovers as a predetermined dominant mechanism. Third, at the empirical and governance level, the study provides evidence from the Guanzhong Plain Urban Agglomeration, a semi-arid and ecologically fragile urban region in the Yellow River Basin. This case allows us to examine how water scarcity, soil erosion risk, industrial pressure, human capital differences, fiscal capacity, and ecological governance jointly shape resilience trajectories. The findings therefore offer policy-relevant evidence for stage-sensitive and place-based resilience governance in ecologically constrained urban agglomerations.

2. Method

2.1. Research Framework

This study develops a layered, mechanism-oriented framework to identify the drivers of urban ecological resilience (UER) in the Guanzhong Plain Urban Agglomeration (Figure 1). Building on adaptive resilience theory and evolutionary urban systems perspectives, the framework conceptualizes resilience drivers as inherently non-static, with associations and elasticities that vary across development stages and spatial contexts. The framework links four components: empirical foundation, robust driver screening, non-static mechanism analysis, and governance interpretation.

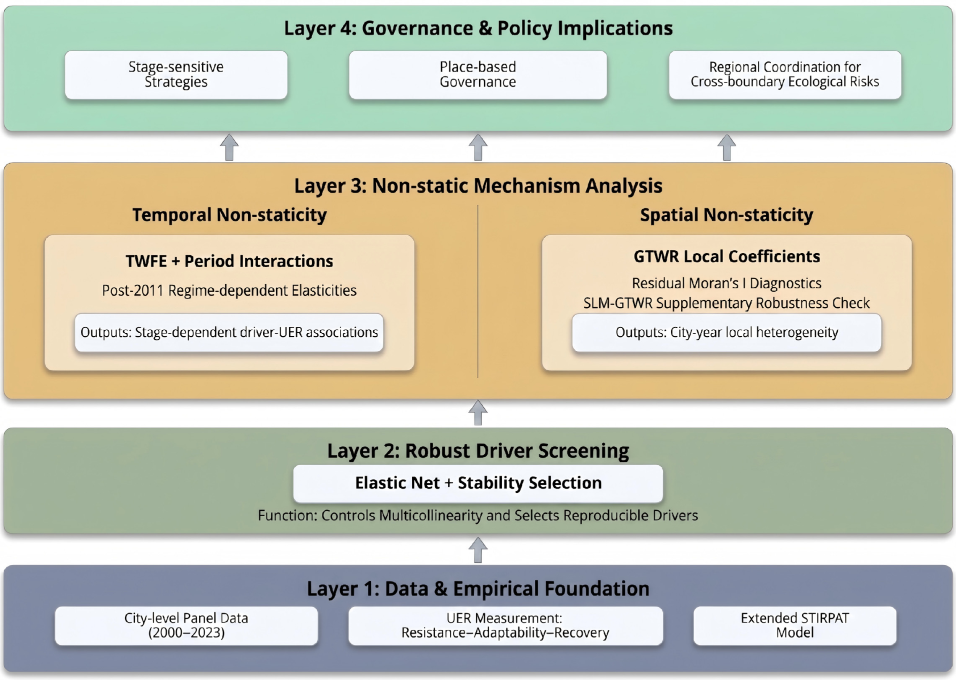

Figure 1. Research framework and analytical strategy for urban ecological resilience.

At the empirical base, we construct a city-level panel for 2000–2023 and operationalize UER through three dimensions—resistance, adaptability, and recovery—within an extended STIRPAT framework [6,7].

To address high dimensionality and multicollinearity, Elastic Net regularization combined with stability selection is used to identify a parsimonious set of robust drivers [13,17].

The analytical core examines the non-static nature of resilience formation along two complementary dimensions. Temporal non-staticity refers to changes in conditional driver–UER elasticities across development stages and policy regimes. It is assessed using two-way fixed-effects specification with period interactions to detect post-2011 structural shifts and regime-dependent changes in resilience drivers.

Spatial non-staticity refers to geographical variations in driver effectiveness arising from differences in economic structures, resource endowments, and governance capacities across cities. It is examined primarily through GTWR, which estimates city-year-specific local coefficients after variable reduction and thereby captures continuous local spatiotemporal heterogeneity in resilience–driver relationships. Residual spatial dependence is then diagnosed using Moran's I under a baseline k = 3 nearest-neighbor spatial weights matrix and alternative k = 4, k = 5, and inverse-distance specifications. SLM-GTWR is retained as a supplementary spatial-lag robustness specification to examine whether the main GTWR coefficient patterns remain stable after introducing a spatial-lag term, rather than as the primary basis for claiming strong spatial spillover effects [12,18–20].

Finally, the framework translates these temporal and spatial mechanisms into governance-relevant insights, treating resilience as a dynamic, adaptive process characterized by stage-dependent and place-specific driver associations [2,16]. Accordingly, the framework links driver identification to adaptive governance by revealing how resilience determinants evolve across time and space and by providing evidence for stage-sensitive and place-based policy interventions, supported by regional coordination where ecological functions, infrastructure networks, public services, and environmental risks cross administrative boundaries.

2.2. Research Area and Data Sources

2.2.1. Research Area

The Guanzhong Plain Urban Agglomeration (GPUA) is located in central China (33°21′–36°43′ N, 104°34′–112°12′ E) and comprises 11 prefecture-level cities across Shaanxi, Shanxi, and Gansu provinces, with Xi'an as the core metropolitan center (Figure 2). Bounded by the Qinling Mountains to the south and the Loess Plateau to the north, the region forms a transitional zone with pronounced topographic and ecological gradients [21,22]. This geographical setting makes the GPUA not only an important urban development corridor in western China, but also a sensitive ecological transition zone between mountain ecosystems, loess hilly–gully landscapes, and semi-arid inland basins.

The GPUA is a typical semi-arid and ecologically fragile region in the Yellow River Basin. Its ecological background is characterized by limited water availability, uneven precipitation, high evapotranspiration, fragile loess landforms, and long-term soil erosion risks. The northern part of the region is closely connected with the Loess Plateau, where soil erosion and vegetation degradation have historically constrained ecosystem stability, while the central plain area faces increasing pressure from intensive urban construction, agricultural production, and water demand. These natural constraints mean that the ecological resilience of the GPUA is highly sensitive to land-use conversion, water-resource stress, landscape fragmentation, and changes in ecological service provision.

The GPUA occupies a strategic position in western China as both a growth pole and an ecological transition zone. As a key node of the Belt and Road Initiative and the Yellow River Basin, it plays an important role in regional coordination, westward opening, and ecological protection under the high-quality development agenda [23]. At the same time, rapid urbanization and industrial expansion have intensified land-use conversion, resource consumption, and environmental stress. By 2020, the region hosted approximately 38.9 million permanent residents and generated a regional GDP of about CNY 2.2 trillion [24]. These characteristics make the GPUA a representative case for examining the spatiotemporal dynamics of urban ecological resilience and its drivers in a rapidly transforming but ecologically constrained urban system [3,25]. The coexistence of rapid urban growth, water scarcity, soil erosion risk, and ecological protection responsibilities creates a typical tension between development expansion and ecological resilience maintenance.

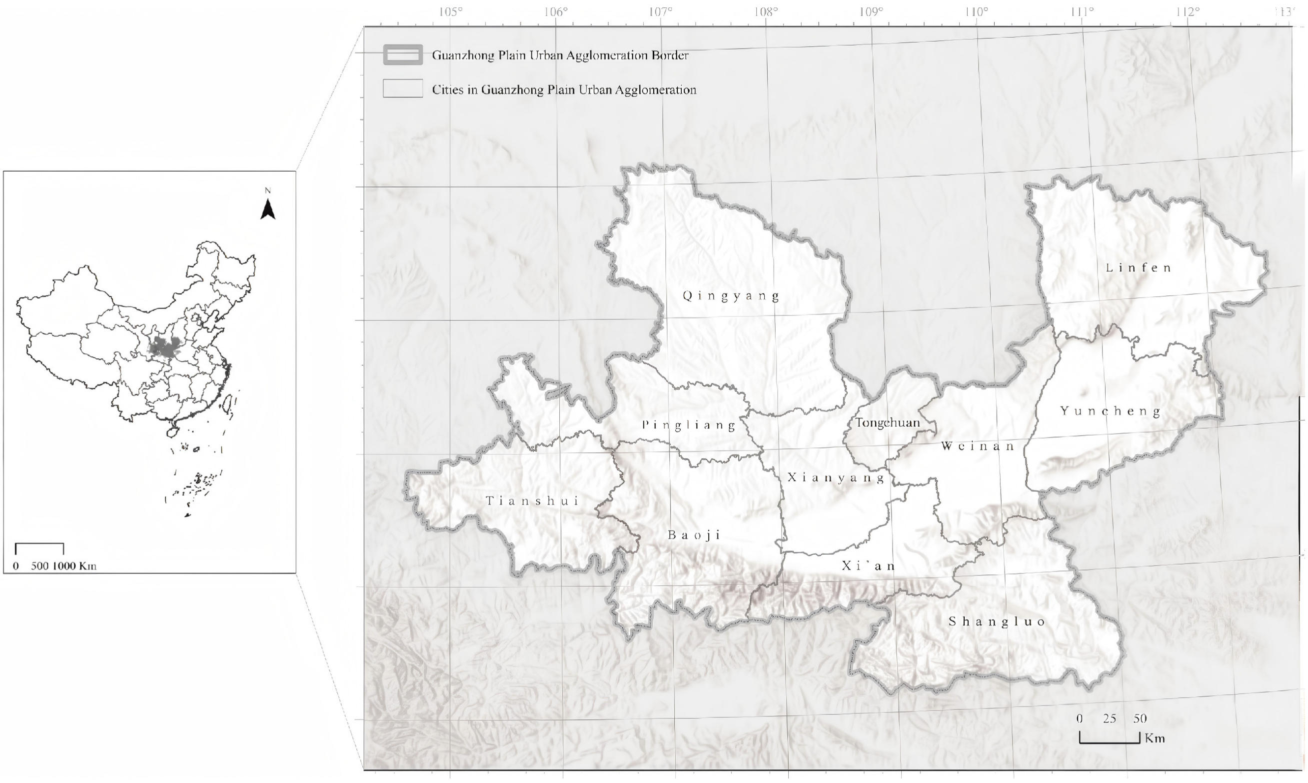

Figure 2. Location of the Guanzhong Plain Urban Agglomeration and its constituent prefecture-level cities.

Findings from this setting offer policy-relevant evidence for resilience governance in the Yellow River Basin and similar ecologically constrained regions.

2.2.2. Data Sources and Processing

This study integrates statistical and geospatial datasets to construct a prefecture-level panel for the Guanzhong Plain Urban Agglomeration covering 2000–2023. Land-use/land-cover (LULC) data were obtained from the 30 m resolution dataset developed by Yang and Huang (2021) [12], which classifies land use into six major categories according to established Chinese standards [26,27]. Grain production, sown area, and agricultural product prices were compiled from the China Regional Economic Statistical Yearbook, city statistical yearbooks, and the National Compilation of Agricultural Product Costs and Returns [28]. Demographic, social development, and industrial structure indicators were collected from the China City Statistical Yearbook and official municipal statistical sources.

City-level energy consumption and carbon-related indicators were compiled following established accounting frameworks. Energy–carbon conversion was based on the IPCC Guidelines for National Greenhouse Gas Inventories [29], supplemented by prefecture-level accounting practices commonly used in the Chinese context [30,31]. City-level CO_2 emissions were drawn from the China Energy Statistical Yearbook (2000–2023). All source data were harmonized by city, administrative unit, and year before being merged into a unified prefecture-level city-year panel. LULC data were clipped to prefecture-level city boundaries, and land-use areas were calculated by land-use category to support the construction of the ESV-based resistance and land-use recovery indicators. Statistical variables were aggregated or matched to the prefecture-city level to ensure comparability and consistency across cities and years.

To improve reproducibility, missing values were treated at the city–variable time-series level. Specifically, missing observations in continuous socioeconomic variables were first checked by city and variable. Isolated missing values within a city-specific time-series were filled using linear interpolation between adjacent observed years to preserve temporal continuity [32]. After interpolation and consistency checks, the final modeling dataset contained 264 city–year observations, covering 11 prefecture-level cities from 2000 to 2023. Although this procedure preserves temporal continuity in the city-level panel, it may smooth short-term fluctuations and weaken the detection of abrupt annual changes. Therefore, the results should be interpreted primarily as long-term trends and conditional associations rather than as precise estimates of short-term shocks.

Before model estimation, monetary variables were adjusted to constant 2000 prices where applicable to ensure temporal comparability. Continuous explanatory variables were winsorized at the 1st and 99th percentiles to reduce the influence of extreme values. A small positive constant was added where necessary before logarithmic transformation to avoid undefined logarithms for zero or near-zero values. The log-transformed variables were then used in the subsequent TWFE-STIRPAT, Elastic Net, GTWR, and SLM-GTWR analyses, with additional standardization or two-way demeaning applied in the corresponding modeling steps described below.

2.3. Measuring Urban Ecological Resilience (UER) in the Guanzhong Plain Urban Agglomeration

Ecological resilience was originally conceptualized by Holling (1973) [33] as the capacity of ecosystems to absorb disturbances and reorganize while retaining essential structures and functions. This perspective has subsequently been extended to social–ecological and urban systems, in which resilience is commonly understood as comprising the capacities to resist or absorb shocks, adapt to changing conditions, and recover after disturbance [3,15]. Building on the tri-dimensional framework of resistance–adaptability–recovery [14,34,35], we construct a city-year assessment framework for the Guanzhong Plain Urban Agglomeration. The three dimensions are denoted as resistance (P), adaptability (A), and recovery (R), respectively.

In this study, urban ecological resilience is conceptualized as the capacity of an urban social–ecological system to withstand external disturbances, adjust its internal spatial structure and ecological functions, and recover ecological performance after disturbance. Accordingly, the three dimensions represent different stages of the resilience process (Table 1). Resistance captures the capacity to withstand or absorb disturbance while maintaining essential ecological functions; adaptability captures the capacity to reorganize and adjust under persistent or cumulative pressures; and recovery captures the capacity to restore ecological performance or move toward a new stable state after disturbance.

It should be noted that the selected indicators are not treated as direct substitutes for the theoretical concepts themselves. Rather, they are used as empirical proxies for theoretically defined resilience processes. Specifically, ecosystem service value (ESV) is used as a proxy for ecological functional maintenance and buffering capacity; landscape stability derived from heterogeneity and fragmentation is used as a proxy for adaptive structural capacity; and area-weighted land-use recovery coefficients are used as a proxy for post-disturbance restoration capacity. This process-based interpretation clarifies the conceptual link between disturbance, adaptive capacity, recovery, and the empirical measurement of UER.

Table 1. Conceptual definitions and empirical proxies of the three UER dimensions.

Dimension	Conceptual Meaning	Resilience Process	Empirical Proxy	Interpretation
Resistance (P)	Ability to maintain essential ecological structures and service functions under external disturbance	Withstanding or absorbing disturbance	Ecosystem service value (ESV)	Ecological functional maintenance and buffering capacity
Adaptability (A)	Ability to adjust spatial structure and functional organization under changing or cumulative pressures	Reorganization and structural adjustment	Landscape stability derived from heterogeneity and fragmentation	Adaptive structural capacity
Recovery (R)	Ability to restore ecological function or move toward a new stable state after disturbance	Post-disturbance restoration and functional rebound	Area-weighted land-use recovery coefficients	Restorative capacity of the ecological land-use structure

Notes: The indicators listed in the "Empirical proxy" column are not treated as direct equivalents of the theoretical dimensions. Instead, they are used to operationalize theoretically defined resilience processes in a city-year empirical framework.

2.3.1. Resistance (*P*): Ecosystem Service Value as a Proxy for Ecological Buffering Capacity

Resistance refers to the ability of an urban ecological system to absorb external pressures while maintaining essential ecological structures and service functions. In rapidly urbanizing regions, major disturbances arise from land conversion, population concentration, infrastructure expansion, and intensified resource consumption. Therefore, resistance is not measured by disturbance exposure itself, but by the system's capacity to maintain ecological functions under these pressures.

In this study, ecosystem service value (ESV) is used as an empirical proxy for ecological buffering capacity rather than as resistance itself; higher ESV indicates stronger functional support and greater capacity to maintain service provision under disturbance. We proxy resistance using ecosystem service value (ESV), computed with the widely adopted equivalent factor (unit-area coefficient) method [6,36–38]. Specifically, for city *c* in year *t*

$$P_{c,t} \equiv ESV_{c,t} = \sum_{k=1}^{K} A_{c,t,k} \cdot VC_{c,k} \quad (1)$$

where $A_{c,t,k}$ denotes the area (hm^2) of land-use type k, and $VC_{c,k}$ represents the unit-area ESV coefficient ($CNY \cdot hm^{-2} \cdot yr^{-1}$). Coefficients for Xi'an and the other cities are reported in Tables 2 and 3, following localized revisions consistent with the equivalent factor framework [38].

Table 2. Ecosystem service value (ESV) coefficients by land-use type and ecosystem service function in Xi'an ($CNY \cdot hm^{-2} \cdot yr^{-1}$).

Ecosystem Services and Functions	Farmland	Forest	Grassland	Water	Wetland	Bare Land	Build-Up Land
Gas exchange	938.59	6570.15	1501.75	0.00	3378.94	0.00	0
Climate regulation	1670.70	5068.40	1689.47	863.51	32,099.90	0.00	0
Water conservation	1126.31	6007.00	1501.75	38,294.61	29,096.40	56.32	0
Soil formation and protection	2740.69	7321.03	3660.51	18.77	3209.99	37.54	0
Waste disposal	3078.59	2459.11	2459.11	34,164.80	34,127.25	18.77	0
Biodiversity conservation	1332.80	6119.63	2046.13	4674.19	4692.97	638.24	0
Food production	1877.19	187.72	563.16	187.72	563.16	18.77	0
Raw material	187.72	4880.69	93.86	18.77	131.40	0.00	0

Table 2. *Cont.*

Ecosystem Services and Functions	Farmland	Forest	Grassland	Water	Wetland	Bare Land	Build-Up Land
Entertainment and leisure	18.77	2402.80	75.09	8146.99	10,418.39	18.77	0
Total	12,971.36	41,016.53	13,590.83	86,369.37	117,718.38	788.42	0

Notes: VC_k^c denotes the unit-area ESV coefficient for ecosystem service function s associated with land-use type k ($CNY \cdot hm^{-2} \cdot yr^{-1}$). "Total" reports the coefficient aggregated across ecosystem service functions for each land-use type, i.e., $VC_k = \sum_s VC_k^{(s)}$. Coefficients for built-up land are set to zero, consistent with standard equivalent factor ESV valuation practice, to avoid attributing ecosystem service provision to impervious surfaces. This table provides the function-level decomposition for Xi'an.

Table 3. City-specific unit-area ecosystem service value (ESV) coefficients by land-use type in the Guanzhong Plain Urban Agglomeration ($CNY \cdot hm^{-2} \cdot yr^{-1}$).

City	Farmland	Forest	Grassland	Water	Wetland	Bare Land	Build-Up Land
Baoji	11,186.56	35,372.85	11,720.80	74,485.35	101,520.89	679.94	0
Tongchuan	10,160.47	32,128.25	10,645.70	67,653.12	92,208.80	617.57	0
Xianyang	12,365.43	39,100.53	12,955.96	82,334.80	112,219.41	751.59	0
Weinan	10,656.96	33,698.21	11,165.91	70,959.02	96,714.63	647.75	0
Shangluo	7913.78	25,024.04	8291.72	52,693.64	71,819.56	481.01	0
Yuncheng	11,188.96	35,380.42	11,723.31	74,501.28	101,542.61	680.08	0
Linfen	10,788.43	34,113.93	11,303.65	71,834.41	97,907.75	655.74	0
Tianshui	8754.17	27,681.42	9172.24	58,289.35	79,446.32	532.09	0
Pingliang	8096.78	25,602.70	8483.46	53,912.15	73,480.35	492.13	0
Qingyang	7907.15	25,003.06	8284.77	52,649.48	71,759.37	480.61	0

Notes: $VC_{c,k}$ denotes the city-specific unit-area ESV coefficient for land-use type k in city c ($CNY \cdot hm^{-2} \cdot yr^{-1}$), aggregated across ecosystem service functions. Aggregation across ecosystem service functions is defined as $VC_{c,k} = \sum_s VC_{c,k}^{(s)}$, where $VC_{c,k}^{(s)}$ is the unit-area coefficient for function s. The coefficients are used to compute ESV-based resistance (see Equation (1)). Coefficients for built-up land are set to zero, consistent with standard equivalent factor ESV valuation practice, to avoid attributing ecosystem service provision to impervious surfaces.

Accordingly, $P_{c,t}$ should be interpreted as ESV-based resistance, namely the ecological functional maintenance capacity represented by ecosystem service provision, rather than as a direct or exhaustive measure of resistance.

It should be noted that the ESV coefficients provide a comparable proxy for ecological functional maintenance, but they may not fully capture local differences in ecosystem quality, soil–water conditions, species composition, or management intensity within the Guanzhong Plain.

2.3.2. Adaptability (A): Landscape Stability Derived from Heterogeneity and Fragmentation

Adaptability refers to the capacity of an urban system to accommodate disturbances through structural adjustment and spatial reorganization [14]. In the context of urban ecological resilience, adaptability emphasizes whether the landscape pattern can support ecological connectivity, functional complementarity, and structural flexibility under persistent or cumulative disturbances. A more heterogeneous and structurally stable landscape can provide multiple ecological pathways and alternative functional spaces, whereas excessive fragmentation may weaken connectivity and reduce the system's ability to adjust to changing conditions.

We construct the adaptability index $A_{c,t}$ using landscape-level metrics derived from LULC maps in FRAGSTATS v4.3 [39]. Specifically, adaptability is operationalized by two equally weighted components: landscape heterogeneity and landscape fragmentation (Table 4). Heterogeneity is measured by Shannon's diversity index [40] and the area-weighted mean patch fractal dimension [41], while fragmentation is measured by patch density [42].

Table 4. Landscape metrics, expected directions, and weights used to construct the adaptability index.

Dimension	Metric	Abbreviation	Direction	Weight	Software
Landscape heterogeneity	Shannon's diversity index	SHDI	+	0.25	FRAGSTATS
Landscape heterogeneity	Area-weighted mean patch fractal dimension	AWMPFD	+	0.25	FRAGSTATS
Landscape fragmentation	Patch density	PD_L	−	0.50	FRAGSTATS

Notes: Landscape metrics are derived from LULC maps using FRAGSTATS (v4.3). "Direction" indicates the expected monotonic relationship with adaptability: "+" denotes higher metric values imply higher adaptability, whereas "−" denotes higher values imply lower adaptability; the fragmentation-related metric is reverse-coded during index construction using min–max normalization (see Equation (2)). Weights assign equal contributions to landscape heterogeneity (0.50 in total; SHDI and AWMPFD, 0.25 each) and fragmentation/connectivity (0.50). The adaptability index represents the adaptive structural capacity of the ecological landscape, with heterogeneity reflecting functional diversity and fragmentation reflecting constraints on connectivity and spatial reorganization. In Equation (2), the tilde symbol denotes min–max normalization over the full city–year sample. Since higher PD indicates stronger fragmentation and lower adaptability, PD is reverse-coded as $1 - \widetilde{\mathrm{PD}}_{\mathrm{c,t}}$ before aggregation.

Because higher PD indicates stronger fragmentation and thus lower adaptability, PD is reverse-coded in index construction [6]. After min–max normalization, the adaptability index is calculated as:

$$\boldsymbol{A_{c,t}} = \mathbf{0.25}\,\boldsymbol{S\hat{H}DI_{c,t}} + \mathbf{0.25}\,\boldsymbol{AW\hat{M}PFD_{c,t}} + \mathbf{0.50}\left(1 - \boldsymbol{P\hat{D}\_L_{c,t}}\right) \tag{2}$$

where $\boldsymbol{A_{c,t}}$ denotes the adaptability index for city $\boldsymbol{c}$ in year $\boldsymbol{t}$; $\boldsymbol{SHDI_{c,t}}$, $\boldsymbol{AWMPFD_{c,t}}$, and $\boldsymbol{PD\_L_{c,t}}$ denote Shannon's diversity index, area-weighted mean patch fractal dimension, and patch density, respectively. The tilde symbol ($\sim$) indicates the min–max normalized value of each landscape metric over the full city-year sample. Thus, $\boldsymbol{S\widetilde{H}DIc, t}$, $\boldsymbol{AW\widetilde{M}PFDc, t}$, and $\boldsymbol{P\widetilde{D}\_Lc, t}$ represent the normalized values of SHDI, AWMPFD, and PD for city $\boldsymbol{c}$ in year $\boldsymbol{t}$. Because higher $\boldsymbol{PD}$ indicates stronger landscape fragmentation and lower adaptability, $\mathbf{1} - \boldsymbol{P\widetilde{D}\_Lc, t}$ is used as the reverse-coded fragmentation/connectivity component. The weights 0.25, 0.25, and 0.50 correspond to the baseline contributions of SHDI, AWMPFD, and reverse-coded PD_L in the adaptability index. Details of the metric definitions, expected directions, and weights are reported in Table 4.

The baseline weighting scheme is concept-based rather than data-fitted. It assigns equal conceptual importance to two non-substitutable components of adaptive structural capacity: landscape heterogeneity and landscape fragmentation/connectivity. Specifically, ***SHDI*** and ***AWMPFD*** jointly represent landscape heterogeneity and are assigned a combined weight of 0.50, with each metric receiving 0.25. Reverse-coded ***PD_L*** represents landscape fragmentation/connectivity and is assigned a weight of 0.50. This design ensures that the adaptability index gives balanced importance to landscape diversity and spatial connectivity, which together shape the capacity of the ecological landscape to reorganize under disturbance.

Thus, $\boldsymbol{A_{c,t}}$ should be interpreted as a landscape stability-based proxy for adaptive structural capacity. It does not capture all institutional or socioeconomic aspects of adaptability, but focuses on the ecological and spatial-structural capacity of the urban landscape to reorganize under disturbance.

2.3.3. Recovery (R): Area-Weighted Land-Use Recovery Coefficients

Recovery characterizes a system's capacity to restore, or reorganize toward, a stable state following disturbances. Unlike resistance, which emphasizes the ability to withstand disturbance, recovery focuses on post-disturbance restoration and functional rebound. In urbanizing regions, recovery is closely related to whether ecological land and associated ecological functions can be restored after land-use conversion, infrastructure expansion, or other cumulative disturbances.

Following coefficient-based approaches widely used in land-use resilience and ecosystem health assessments, we assign each land-use type a recovery coefficient, $RC_k \in [0,\ 1]$, and compute the recovery index as an area-weighted mean:

$$R_{c,t} = \sum_{k=1}^{K} \left(\frac{A_{c,t,k}}{\sum_{k=1}^{K} A_{c,t,k}} \right) \cdot RC_k \tag{3}$$

where $\mathbf{A_{c,t,k}}$ denotes the area of land-use type **k** in city **c** at year **t**, and **K** is the total number of land-use categories. The recovery coefficients are harmonized to the LULC typology adopted in this study based on Peng et al. [43] and subsequent applications under comparable classification schemes. The adopted $\mathbf{R_{c,t}}$ values and the corresponding cross-walk rules are summarized in Table 5.

Table 5. Land-use recovery coefficients (RC_k) used to construct the recovery index ($R_{c,t}$).

Land-Use Type	Abbrev.	RC_k	Source
Cropland (Farmland)	CRO	0.30	[43,44]
Forest	FOR	0.80	[43,44]
Grassland	GRA	0.60	[44]
Water bodies	WAT	0.80	[43,44]
Wetland	WET	0.80	[44]
Unused/Bare land	UNL	1.00	[43,44]
Built-up land	BUL	0.20	[43,44]

Notes: $RC_k \in [0,\ 1]$, where higher values indicate stronger recovery potential for land-use type k. The recovery index is computed as an area-share–weighted mean of RC_k across land-use types, as shown in Equation (3). Recovery coefficients compiled from the literature are harmonized to the LULC classification adopted in this study through an explicit cross-walk between source categories and the study typology.

In this study, $R_{c,t}$ is interpreted as an empirical proxy for post-disturbance ecological restoration capacity. Higher values indicate that a larger share of the urban land system is composed of land-use types with stronger recovery potential. This indicator therefore captures the restorative capacity of the ecological land-use structure, rather than measuring actual recovery trajectories after a single discrete disturbance event.

Similarly, the recovery coefficients represent literature-based recovery potential by land-use type. Although they are harmonized to the LULC classification used in this study, they cannot fully capture local restoration difficulty, degradation history, or management effectiveness.

2.3.4. Normalization and Composite Construction of the Urban Ecological Resilience Index

Because the three core dimensions—resistance (**P**), adaptability (**A**), and recovery (**R**)—are measured on different scales, each dimension is normalized over the full city–year sample using min–max scaling to ensure comparability [6,45,46]. Specifically

$$z(X_{c,t}) = \frac{X_{c,t} - \mathbf{min}(X)}{\mathbf{max}(X) - \mathbf{min}(X)} \tag{4}$$

where $z(X_{c,t})$ is the normalized value of dimension X for city c in year t, with $X \in [P, A, R]$. Following established practice in urban resilience assessment, the composite UER index is then calculated as the arithmetic mean of the three normalized dimensions:

$$\boldsymbol{UER_{c,t}} \equiv \frac{\mathbf{1}}{\mathbf{3}}[z(\boldsymbol{P_{c,t}}) + z(\boldsymbol{A_{c,t}}) + z(\boldsymbol{R_{c,t}})] \tag{5}$$

The equal-weighted aggregation is adopted as the baseline composite measure for three reasons. First, resistance, adaptability, and recovery represent three theoretically distinct but equally essential stages of the resilience process: withstanding disturbance, reorganizing under changing conditions, and restoring ecological performance after disturbance. Given the absence of a universally accepted theoretical or empirical basis for prioritizing one dimension over the others, equal weighting provides a transparent and parsimonious benchmark. Second, it avoids imposing an arbitrary hierarchy among the three dimensions. Third, the additive aggregation form facilitates comparability with existing multidimensional resilience assessments.

To evaluate whether the composite UER index is sensitive to the internal weighting of the adaptability dimension, we conducted an additional robustness test by replacing the baseline concept-based weights (0.25, 0.25, 0.50) for SHDI, AWMPFD, and reverse-coded PD with an equal-metric scheme (1/3, 1/3, 1/3). The adaptability index and the composite UER index were then recalculated using the same normalization and aggregation procedure. Details of the alternative weighting specification and the corresponding results are provided in Appendix B.

The results indicate that, although the alternative weighting scheme affects the absolute level of the adaptability sub-index, the temporal evolution and overall pattern of the composite UER index remain highly consistent with the baseline results. This suggests that the main findings are not materially driven by the specific weighting configuration adopted in the baseline index. Therefore, the equal-weighted UER index is retained because of its theoretical interpretability, transparency, and demonstrated robustness.

2.4. A STIRPAT-Based Framework for Identifying Non-Static and Spatially Heterogeneous Resilience Drivers

Given the moderate size of the city–year panel, the empirical strategy is designed as a sequential and parsimonious framework rather than as a model-stacking exercise. Each model serves a distinct analytical purpose: Elastic Net reduces the initial driver pool and controls multicollinearity; TWFE estimates average and period-dependent elasticities; GTWR explores local spatiotemporal heterogeneity after variable reduction; residual Moran's I diagnostics assess whether spatial dependence remains under alternative neighborhood and distance-based spatial weights; and SLM-GTWR is retained as a supplementary robustness specification rather than as the primary evidence for spatial spillovers. This sequence is intended to limit model complexity while allowing the analysis to move from robust driver identification to temporal and spatial mechanism interpretation.

2.4.1. Baseline Specification: Two-Way Fixed-Effects STIRPAT Model

To identify the key drivers of urban ecological resilience (UER), we embed the STIRPAT framework in a two-way fixed-effects (TWFE) panel model. In line with the objective of this study, the model is used to examine conditional associations and elasticity heterogeneity between UER and potential socioeconomic drivers, rather than to establish strict causal effects. This specification allows us to examine how anthropogenic factors are associated with UER over time while controlling for unobserved city-specific heterogeneity and common time shocks [20,47].

The analysis is based on an unbalanced panel of 11 prefecture-level cities in the Guanzhong Plain Urban Agglomeration from 2000 to 2023. We retain the log-log form of the stochastic STIRPAT model, which enables direct elasticity interpretation [7]:

$$I \equiv aP^bA^cT^de,$$

or, equivalently,

$$\ln I \equiv \alpha + b\ln P + c\ln A + d\ln T + \varepsilon$$

where **I** denotes the environmental outcome of interest, represented here by urban ecological resilience; **P**, **A**, and **T** denote population, affluence, and technology-related factors, respectively [6,48]. All variables are log-transformed. A small positive constant is added where necessary to avoid undefined logarithms, and continuous variables are winsorized at the 1st and 99th percentiles.

The empirical baseline is specified as:

$$\ln UER_{c,t} \equiv \alpha_c + \gamma_t + \sum_{k=1}^{K} \beta_k \ln X_{k,c,t} + \varepsilon_{c,t} \quad (6)$$

where $\mathbf{UER_{c,t}}$ is the urban ecological resilience index for city **c** in year **t**, α_c and γ_t denote city and year fixed-effects, respectively, and β_k captures the elasticity of the **k**-th explanatory variable. Here, β_k is interpreted as a conditional driver–UER elasticity after controlling for city and year fixed-effects, rather than as a causal marginal effect. The model is estimated by ordinary least squares with standard errors clustered at the city level to account for within-city serial correlation and heteroskedasticity [49]. This TWFE-STIRPAT model serves as the global baseline for the subsequent machine-learning screening and heterogeneity analyses.

The empirical models identify non-static associations and local heterogeneity rather than strict causal effects. City and year fixed-effects control for time-invariant city characteristics and common temporal shocks, but cannot fully eliminate time-varying omitted variables, simultaneity, or reverse causality. For example, fiscal investment may be associated with UER because public expenditure supports environmental infrastructure and ecological restoration, but cities with higher ecological resilience may also attract more fiscal resources, and cities with lower resilience may receive compensatory investment. Therefore, the estimated coefficients are interpreted as resilience–driver associations within a spatiotemporal heterogeneity framework, rather than as evidence of one-way causal effects.

2.4.2. Machine-Learning Screening of Resilience Drivers: Elastic Net with Stability Selection

Building on prior resilience and STIRPAT-related studies, we compile an initial pool of 20 candidate drivers spanning four dimensions of urban ecological resilience (Table 6). The social development dimension includes population density (PD), population size (POP), urbanization level (URB), human capital level (HC), education expenditure level (EDU), and medical and health level (MHL), which together capture demographic pressure, urbanization, educational investment, and public-service capacity. The economic development dimension includes GDP growth rate (GDPG), GDP per capita (PGDP), fiscal investment intensity (FI), and trade openness (TO), reflecting short-term economic dynamics, average affluence, state intervention capacity, and external openness. The industrial structure dimension includes the contribution rates of primary, secondary, and tertiary industries to GDP (PRI, SEC, and TER), together with the industrial structure upgrading index (HCI) and the industrial structure advancement indicator (ISA), which capture both compositional structure and upgrading toward service-oriented activities. The environmental carrying capacity and sustainability dimension includes per capita energy consumption (PCEC), energy intensity (EI), carbon emissions per unit of energy consumption (CEI), total energy consumption (TEC), and total carbon dioxide emissions (CDE), thereby covering the scale, efficiency, intensity, and outcome aspects of energy use and carbon emissions. Detailed definitions and units are reported in Table 5.

Table 6. Candidate drivers of urban ecological resilience in the extended STIRPAT framework.

Dimension	Candidate Variable	Abbrev.	Unit	Definition
Social Development	Population Density	PD	persons/km^2	Number of residents per square kilometer, capturing the intensity of population pressure.
	Population Size	POP	persons	Total resident population, reflecting the scale effect of population size.
	Urbanization Level	URB	%	Share of non-agricultural (urban) population in total population, indicating the level of urbanization.
	Human Capital Level	HC	%	Share of students enrolled in regular higher-education institutions in the total population; proxy for higher-education attainment and local human capital accumulation capacity.
	Education Expenditure Level	EDU	%	Ratio of education expenditure to total public budget expenditure, capturing fiscal commitment to education.
	Medical and Health Level	MHL	beds/100 persons	Number of hospital or health-institution beds per 100 persons, indicating public health-service capacity.
Economic Development	GDP Growth Rate	GDPG	%	Annual real GDP growth rate, capturing short-term economic dynamics.
	GDP per Capita	PGDP	CNY/person	Gross domestic product divided by total population, reflecting average economic affluence.
	Fiscal Investment Intensity	FI	%	Ratio of fixed-asset investment to total public budget expenditure, reflecting macro-level policy intervention capacity.
	Trade Openness	TO	%	Ratio of actually utilized foreign direct investment (FDI) to GDP, measuring the degree of external openness.
Industrial Structure	Contribution Rate of Primary Industry to GDP	PRI	%	Share (contribution) of primary industry value added in GDP.
	Contribution Rate of Secondary Industry to GDP	SEC	%	Share (contribution) of secondary industry value added in GDP.
	Contribution Rate of Tertiary Industry to GDP	TER	%	Share (contribution) of tertiary industry value added in GDP.
	Industrial Structure Upgrading Index	HCI	%	Weighted sum of sectoral shares with increasing weights assigned to primary–secondary–tertiary industries; higher values indicate a more service-oriented structure.
	Industrial Structure Advancement	ISA	ratio	Ratio of tertiary to secondary industry value added; higher values indicate upgrading toward an advanced (service-led) structure.
Environmental Carrying Capacity & Sustainability	Per capita energy consumption	PCEC	tce/person	Energy consumption per person (tce = tons of coal equivalent).
	Energy Intensity	EI	tce/10^4 CNY	Energy consumption per unit of GDP, capturing energy use efficiency.
	Carbon Emissions per Unit Energy Consumption	CEI	t CO_2/10^4 tce	CO_2 emissions per unit of energy consumption, reflecting carbon intensity of the energy structure.
	Total Energy Consumption	TEC	tce	Total final energy consumption, capturing the scale effect of energy use.
	Carbon Dioxide Emissions	CDE	t CO_2	Total CO^2 emissions associated with energy consumption.

Notes: CNY denotes Chinese yuan; tce denotes tons of coal equivalent; ratio indicates a dimensionless indicator. This table reports the initial candidate pool (20 variables) compiled from resilience- and STIRPAT-related studies and adapted to data availability for the Guanzhong Plain Urban Agglomeration. Environmental variables are designed to capture different mechanisms: TEC reflects the scale of energy use, PCEC and EI capture energy use efficiency, and CEI and CDE represent carbon intensity and emission outcomes, respectively. "Abbrev." denotes the variable abbreviation used in the empirical models; units are reported in their observed form prior to transformation. Monetary values are adjusted to constant 2000 prices to ensure temporal comparability.

This candidate pool is intended to capture the multidimensional mechanisms underlying urban ecological resilience. A central challenge in extended STIRPAT applications is that the affluence (**A**) and technology (**T**) components are often proxied by multiple socioeconomic and structural indicators that are highly correlated, which may lead to multicollinearity and unstable coefficient estimates [8]. To obtain a parsimonious and reproducible driver set while preserving the interpretability of the STIRPAT framework, we combine Elastic Net regularization with stability selection [13,17]. Post-selection estimation is then conducted within the two-way fixed-effects (TWFE) framework [50].

Step 1. Two-way demeaning and standardization.

We begin with the logged dependent variable, ln$\mathbf{UER_{c,t}}$, and the logged covariates, ln$\mathbf{X_{k,c,t}}$. To ensure that variable selection targets the same identifying variation as the TWFE estimator, all variables are first transformed by two-way demeaning at the city and year levels, thereby partialling out city and time fixed-effects ($\boldsymbol{\alpha_c}$, $\boldsymbol{\gamma_t}$) [20,51]. The demeaned covariates are then standardized using z-scores so that penalization is comparable across variables and selection is not driven by scale differences [52].

Step 2. Elastic Net pre-screening.

Using the preprocessed data, we estimate an Elastic Net model that combines the $\mathbf{L_2}$ (ridge) penalty, which is effective in handling collinearity, with the $\mathbf{L_1}$ (lasso) penalty, which promotes sparsity. Relative to pure lasso, Elastic Net is better suited to groups of correlated covariates and can retain variables that jointly proxy the latent **A** and **T** mechanisms in STIRPAT [13]. The regularization parameter $\boldsymbol{\lambda}$ is selected using 10-fold cross-validation on the two-way-demeaned and standardized variables. Specifically, the value of λ that minimizes the cross-validated prediction error is used to obtain the initial set of predictors with non-zero coefficients. This ensures that variable selection is based on within-city, over-time variation after removing city and year fixed-effects, while standardization prevents variables with larger scales from being favored during penalization.

Step 3. Stability selection and construction of the robust driver set.

To reduce sensitivity to a single sample split and improve reproducibility, we implement stability selection [17]. Specifically, we conduct $\mathbf{B} = \mathbf{200}$ repeated subsampling runs, each time drawing 75% of the observations, refitting the Elastic Net model, and recording whether each variable is selected. Selection frequencies, denoted by $\boldsymbol{\pi_j}$, are then computed for all candidate drivers.

Variables with $\boldsymbol{\pi_j} \geq \mathbf{0.60}$ are retained as the final robust driver set, $\mathbf{X_{final}}$. The threshold of 0.60 is selected as a moderate and pre-specified retention rule that balances inclusiveness and parsimony in a relatively small city-year panel. A much lower threshold would increase the risk of retaining unstable predictors, whereas a very high threshold could exclude substantively important drivers whose effects may be heterogeneous across cities and periods. Therefore, the selection frequency π_j is interpreted as an indicator of reproducibility rather than as a conventional statistical significance test.

To examine whether the retained driver set is sensitive to the threshold choice, we further conduct threshold sensitivity checks using more stringent cut-offs, including $\pi_j \geq \mathbf{0.65}$, $\pi_j \geq \mathbf{0.70}$, $\pi_j \geq \mathbf{0.75}$, and $\pi_j \geq \mathbf{0.80}$. The results are reported in Appendix E. These checks assess whether the key retained drivers remain stable under alternative selection rules and help ensure that subsequent TWFE, GTWR, and SLM-GTWR analyses are not driven by an arbitrary threshold choice.

Compared with ad hoc stepwise regression or purely unsupervised dimension-reduction methods such as principal component analysis, this procedure preserves the interpretive structure of STIRPAT while delivering a parsimonious predictor set for subsequent post-selection estimation and heterogeneity analysis [50].

The resulting $\mathbf{X_{final}}$ is subsequently introduced into the TWFE-based period heterogeneity specification to examine whether the estimated resilience elasticities exhibit statistically meaningful shifts across policy regimes. This post-selection design ensures that the subsequent TWFE, GTWR, and SLM-GTWR models are estimated using only a reduced set of stability-selected drivers rather than the full candidate pool, thereby reducing the risk that later-stage results are driven by redundant variables or sample-specific noise.

2.4.3. Testing Stage Shifts in Resilience–Driver Elasticities: Period Heterogeneity Analysis

To examine whether the effects of key drivers on urban ecological resilience (UER) vary across policy regimes, we test for period heterogeneity around 2011. The year 2011 is used as a theoretically informed baseline breakpoint rather than as an assumed instantaneous policy shock. It marks the beginning of China's Twelfth Five-Year Plan period, during which resource constraints, energy intensity control, ecological environmental protection, and high-quality development became more systematically embedded in national and regional governance. For the Guanzhong Plain Urban Agglomeration, located in the ecologically fragile Yellow River Basin, this transition is particularly relevant because it reshaped the institutional context through which fiscal investment, energy use, public services, and industrial transformation affected ecological resilience.

Nevertheless, we recognize that policy transitions are gradual rather than occurring at a single date. Therefore, the post-2011 indicator should be interpreted as a parsimonious approximation of a broader governance-regime transition rather than as the exact timing of a discrete policy intervention. To examine whether the period heterogeneity results are sensitive to the specific choice of the 2011 breakpoint, we further conducted alternative breakpoint robustness checks using 2010, 2012, 2013, and 2014 as additional cut-off years. The same stability-selected driver set was retained across all specifications to ensure comparability. The detailed results are reported in Appendix C.

Building on the TWFE-STIRPAT baseline, we interact each robust driver selected in Section 2.4.2 with a post-2011 indicator. Specifically, we define

$$\boldsymbol{Post_t} \equiv \begin{cases} \mathbf{1}, & \boldsymbol{t} \geq \mathbf{2011} \\ \mathbf{0}, & \boldsymbol{t} < \mathbf{2011} \end{cases}$$

Let $\mathbf{X_{k,c,t}}$ denote the $\mathbf{k}$-th driver in the final robust driver set, $\mathbf{X_{final}}$. The period heterogeneity specification is given by:

$$\mathbf{ln}\boldsymbol{UER_{c,t}} = \boldsymbol{\alpha_c} + \boldsymbol{\gamma_t} + \sum\nolimits_{k\in X_{final}} \boldsymbol{\beta_k}\mathbf{ln}\boldsymbol{X_{k,c,t}} + \sum\nolimits_{k\in X_{final}} \boldsymbol{\delta_k}(\mathbf{ln}\boldsymbol{X_{k,c,t}} \times \boldsymbol{Post_t}) + \boldsymbol{\mu_{c,t}} \tag{7}$$

where $\boldsymbol{\beta_k}$ captures the average elasticity in the pre-2011 regime, and $\boldsymbol{\delta_k}$ measures the post-2011 shift in that elasticity. Accordingly, the post-2011 elasticity for driver $\mathbf{k}$ is given by $\boldsymbol{\beta_k} + \boldsymbol{\delta_k}$. This parameterization provides a transparent test of whether the resilience–driver relationship changed after 2011, with the null hypothesis $\mathbf{H_0} : \boldsymbol{\delta_k} = \mathbf{0}$, while continuing to control for time-invariant city heterogeneity ($\boldsymbol{\alpha_c}$) and common temporal shocks ($\boldsymbol{\gamma_t}$) through the two-way fixed-effects structure [20].

The model is estimated by OLS with city-clustered robust standard errors to account for within-city serial correlation and heteroskedasticity over time [49]. For ease of interpretation, we report both the estimated $\boldsymbol{\delta_k}$ coefficients, which capture structural shifts, and the implied post-2011 elasticities, $\boldsymbol{\beta_k} + \boldsymbol{\delta_k}$.

2.4.4. Capturing City–Year Heterogeneity: Geographically and Temporally Weighted Regression (GTWR)

Global models such as OLS and TWFE assume constant elasticities across space and time. This assumption may be restrictive when resilience–driver relationships vary across cities and evolve over time. To capture continuous spatiotemporal heterogeneity beyond the period heterogeneity test in Section 2.4.3, we employ Geographically and Temporally Weighted Regression (GTWR), which allows coefficients to vary jointly over space and time [12].

Let $\mathbf{y_{c,t}}$ denote the standardized logged UER value for city $\mathbf{c}$ in year $\mathbf{t}$, and let $\mathbf{X^*_{k,c,t}}$ denote the logged and standardized value of driver $\mathbf{k}$. The model is specified as:

$$y_{c,t} \equiv \beta_0(u_c, v_c, t) + \sum_k \beta_k(u_c, v_c, t) X^*_{k,c,t} + \varepsilon_{c,t} \tag{8}$$

where $(\mathbf{u_c}, \mathbf{v_c})$ are the coordinates of city $\mathbf{c}$, and $\boldsymbol{\beta}_\mathbf{k}(\mathbf{u_c}, \mathbf{v_c}, \mathbf{t})$ is the city–year-specific local elasticity. GTWR is estimated by locally weighted least squares, with spatiotemporal kernel weights defined as:

$$w_{ij} = \exp\left(-\frac{d^2_{ST,ij}}{2b^2}\right) \tag{9}$$

where $\mathbf{d^2_{ST,ij}}$ is the combined spatiotemporal distance and $\mathbf{b}$ is the bandwidth. An adaptive Gaussian kernel is used, and the spatiotemporal bandwidth is selected using cross-validation rather than AICc minimization [12]. The selected adaptive bandwidth determines the local spatiotemporal neighborhood used for each weighted regression. AICc is reported after estimation as a model comparison and adequacy indicator, but it is not used as the bandwidth-selection criterion. Because the local coefficients are estimated through spatiotemporal smoothing within adaptive neighborhoods, GTWR captures city–year heterogeneity without estimating unrestricted independent regressions for each city–year observation.

We further test residual global spatial dependence using Moran's I. All spatial weights matrices are constructed at the city level and then applied year by year to avoid artificial neighborhood links caused by repeated city–year coordinates. The baseline matrix is a row-standardized (k = 3) nearest-neighbor matrix, which captures local spatial proximity in the 11-city study area. To assess sensitivity to the definition of local-neighborhood structure, we additionally use (k = 4) and (k = 5) nearest-neighbor matrices. To represent geographic distance decay, we also construct an inverse-distance matrix based on centroid-to-centroid distances between cities. All matrices are row-standardized before Moran's (I) testing and SLM-GTWR estimation. If residual spatial autocorrelation is significant, SLM-GTWR is used as a spatial-lag correction [18,30]. If residual spatial autocorrelation is not significant, SLM-GTWR is retained only as a supplementary robustness specification to examine whether the main GTWR coefficient patterns are stable after explicitly incorporating spatial interaction. The detailed results are reported in Appendix D.

2.4.5. Model Validation: Fit, In-Sample Fitted Accuracy, and Residual Spatial Diagnostics

To validate the integrated empirical framework—including the TWFE-STIRPAT baseline, Elastic Net with stability selection, period heterogeneity analysis, and GTWR-based city-year heterogeneity—we assess model performance along three complementary dimensions: goodness-of-fit, in-sample fitted accuracy, and residual diagnostics. This strategy ensures that the results are statistically credible, empirically informative, and transparent with respect to remaining dependence structures, rather than relying solely on in-sample fit when evaluating model adequacy [53].

Because GTWR estimates city–year-specific local coefficient heterogeneity rather than forecasting out-of-sample, we do not apply a random training–testing split, which would disrupt the spatiotemporal neighborhood structure and risk information leakage between adjacent years or neighboring cities. RMSE, MAE, and MAPE are therefore in-sample fitted accuracy metrics computed over the full estimation sample, and the cross-validation step serves only for bandwidth selection.

(1) Goodness-of-fit and model adequacy

For the global panel specifications in Equations (6) and (7), we report $\mathbf{R^2}$ (and adjusted $\mathbf{R^2}$, where appropriate) together with the residual sum of squares (RSS). Inference is based on city-clustered robust standard errors to account for serial correlation and heteroskedasticity within panel units [49]. For the local spatiotemporal model, GTWR adequacy is evaluated using the corrected Akaike Information Criterion (AICc). The adaptive GTWR bandwidth is selected using the cross-validation-based bandwidth criterion described in Section 2.4.4. AICc is reported after model estimation as a model comparison and adequacy indicator, rather than being used as the bandwidth-selection criterion, which is also used to select the optimal bandwidth under the adaptive kernel setting [54].

Because GTWR yields coefficients that vary across both space and time, we further summarize the empirical distribution of local elasticities, $\boldsymbol{\beta_k(u_c, v_c, t)}$, using their mean, standard deviation, and min–max range. Where appropriate, we also compute the coefficient of variation (CV) as a scale-free measure of dispersion:

$$CV_k = \frac{sd(\beta_k(u_c, v_c, t))}{|mean(\beta_k(u_c, v_c, t))|} \tag{10}$$

When the mean coefficient is close to zero, dispersion is interpreted primarily using the standard deviation and min–max range rather than the CV. To demonstrate the robustness of machine-learning-based driver screening, we also report the final retained driver set, $\mathbf{X_{final}}$, together with the selection frequency $\boldsymbol{\pi_j}$ of each retained variable, showing that the selected predictors are not artifacts of a particular subsample or tuning configuration [17]. For transparency and reproducibility, the kernel setting, selected adaptive bandwidth, model fit indicators, and local coefficient summaries are reported in Appendix A.

(2) In-sample fitted accuracy

In-sample fitted accuracy is evaluated using the root mean squared error (RMSE) and mean absolute error (MAE), computed on the log-transformed, two-way demeaned, and standardized outcome $\mathbf{y_{c,t}}$ [55]:

$$RMSE = \sqrt{\frac{1}{N}\sum_{c,t}\left(\hat{y}_{c,t} - y_{c,t}\right)^2},\ MAE = \frac{1}{N}\sum_{c,t}\left|\hat{y}_{c,t} - y_{c,t}\right| \tag{11}$$

where N denotes the number of city–year observations, $y_{c,t}$ denotes the observed transformed UER value, and $\hat{y}_{c,t}$ denotes the fitted value from the GTWR model.

To facilitate interpretation on the original scale, we additionally report the mean absolute percentage error (MAPE) based on the level outcome $\mathbf{UER_{c,t}}$, obtained by back-transforming predictions from the log specification:

$$MAPE = \frac{100}{N}\sum_{c,t}\left|\frac{\hat{UER}_{c,t} - UER_{c,t}}{UER_{c,t}}\right| \tag{12}$$

When MAPE is reported, we ensure $\mathbf{UER_{c,t}} > \mathbf{0}$, or apply the same consistent small-offset rule used prior to log transformation, so as to avoid division issues and maintain comparability across observations. These metrics assess how closely the fitted GTWR values approximate the observed UER values within the estimation sample and should not be interpreted as independent out-of-sample prediction errors.

(3) Residual diagnostics and remaining spatial dependence

Residual behavior is first assessed using standard graphical diagnostics, including residual-versus-fitted plots and Q–Q plots. As a formal test of residual normality, we apply the Shapiro–Wilk test [56]. Given the potential for spatial interactions and shared regional shocks in urban ecological systems, we further examine whether residuals from the local GTWR model exhibit global spatial dependence using Moran's I [57].

Residual Moran's I is calculated annually using a row-standardized k = 3 nearest-neighbor spatial weights matrix as the baseline specification. To assess the sensitivity of the residual spatial diagnostics to the definition of spatial weights, we further conduct robustness checks using k = 4, k = 5, and inverse-distance matrices. Statistical significance is evaluated using permutation tests following standard spatial econometric practice [18].

If significant residual spatial autocorrelation is detected, SLM-GTWR can be used as a spatial-lag correction model. Otherwise, SLM-GTWR is retained only as a supplementary robustness check of whether the main GTWR coefficient patterns remain stable after incorporating a spatial-lag term. In this study, the spatial-lag results are interpreted cautiously as supplementary diagnostic evidence rather than as the primary basis for identifying strong spatial spillover effects.

3. Results

The empirical results are organized according to the sequential logic of the research framework. Section 3.1 first describes the spatiotemporal evolution of UER. Section 3.2 identifies robust drivers and examines temporal non-staticity through period interactions. Section 3.3 focuses on the local spatiotemporal heterogeneity of the key drivers using GTWR, while spatial-lag and alternative spatial weight analyses are reported as supplementary robustness checks.

3.1. Spatiotemporal Evolution of Urban Ecological Resilience

3.1.1. Divergent Trajectories of Resistance, Adaptability, and Recovery

The decomposition of urban ecological resilience (UER) into resistance (P), adaptability (A), and recovery (R) reveals non-synchronous temporal trajectories and clear spatial differentiation across the Guanzhong Plain Urban Agglomeration (GPUA) (Figures 3 and 4). Rather than evolving uniformly, the three components display distinct dynamics, indicating that the region's resilience has been shaped by uneven changes in ecological endowment, landscape restructuring, and land-use recovery capacity.

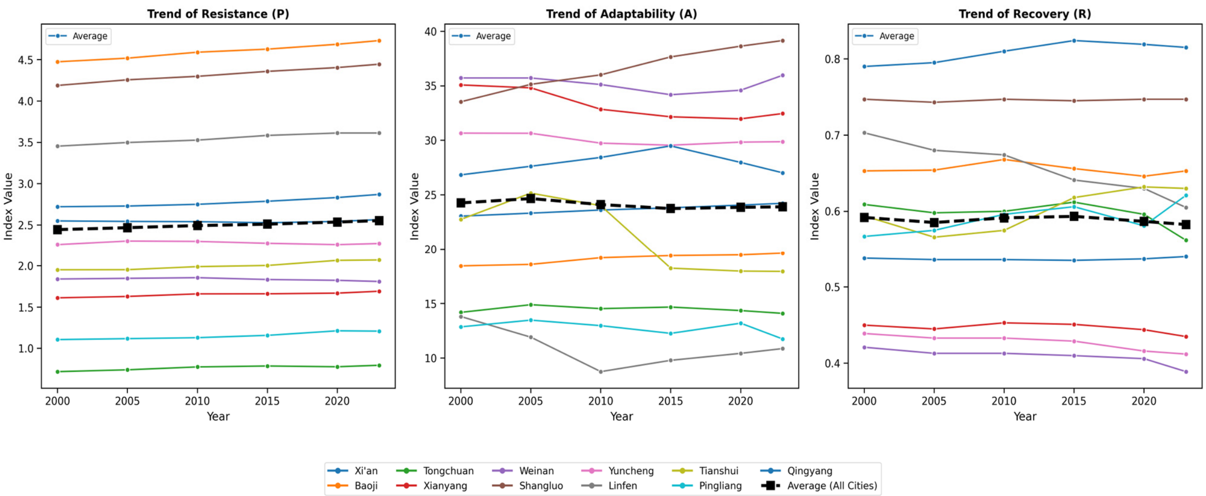

Figure 3. Spatiotemporal trends of the three components of urban ecological resilience—resistance (P), adaptability (A), and recovery (R)—in the Guanzhong Plain Urban Agglomeration from 2000 to 2023.

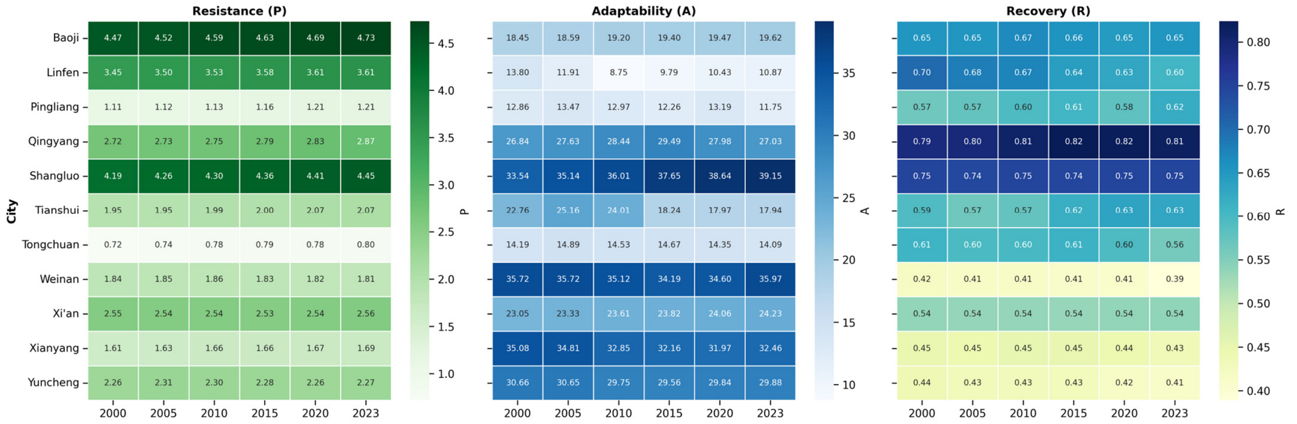

Figure 4. City–year heatmaps of the three sub-dimensions of urban ecological resilience—resistance (P), adaptability (A), and recovery (R)—in the Guanzhong Plain Urban Agglomeration from 2000 to 2023.

At the regional level, resistance (P) shows a modest upward trend over 2000–2023, with the mean increasing from 2.44 to 2.55, suggesting a gradual improvement in the ecosystem service-based resistance dimension. By contrast, recovery (R) declines slightly from 0.61 to 0.60, while inter-city dispersion increases, indicating growing inequality in land-use recovery capacity across cities. Adaptability (A) exhibits the strongest volatility and the widest spread, implying increasingly differentiated pathways of landscape restructuring. Taken together, these patterns suggest that improvements in UER were not uniformly distributed across dimensions, but instead characterized by moderate gains in resistance, relative stagnation in recovery, and intensifying divergence in adaptability.

The spatial heatmaps further highlight substantial inter-city heterogeneity (Figure 4). Resistance (P) shows a relatively stable contrast between ecologically buffered cities and highly urbanized core areas: cities with stronger ecological endowments generally maintain higher resistance levels, whereas heavily urbanized cities remain comparatively low and stable. Adaptability (A) is the most temporally volatile component, indicating greater sensitivity to anthropogenic disturbance and landscape reorganization. Recovery (R) is comparatively more stable and path-dependent, with persistent spatial rankings and only limited temporal change. Overall, resistance (P) and recovery (R) appear to reflect longer-term ecological and land-use conditions, whereas adaptability (A) is more responsive to medium-term human intervention and landscape restructuring.

3.1.2. Overall Spatiotemporal Dynamics of Urban Ecological Resilience

The overall UER index exhibits a pattern of relative aggregate stability accompanied by intensifying spatial differentiation across the GPUA (Figures 5–7). While the regional mean changes only modestly over time, the distributional pattern, spatial hierarchy, and city-specific trajectories reveal increasingly differentiated resilience performance across cities.

The kernel density and boxplot results (Figure 5) show that the regional average level of UER remains relatively stable over 2000–2023, fluctuating around 0.45. By contrast, the cross-city distribution widens over time. The KDE curves become flatter and more dispersed, while the inter-city range expands from 0.535 in 2000 to 0.604 in 2023, indicating increasing heterogeneity in resilience performance despite the relative stability of the regional mean.

The heatmap of city-level UER (Figure 6) reveals a persistent hierarchical structure. Based on average UER levels, cities can be broadly grouped into high-, medium-, and low-resilience tiers, and these relative positions remain fairly stable through time. High-resilience cities consistently occupy the upper end of the distribution, while low-resilience cities remain clustered at the bottom, suggesting persistent structural disparities and limited rank mobility across the urban agglomeration.

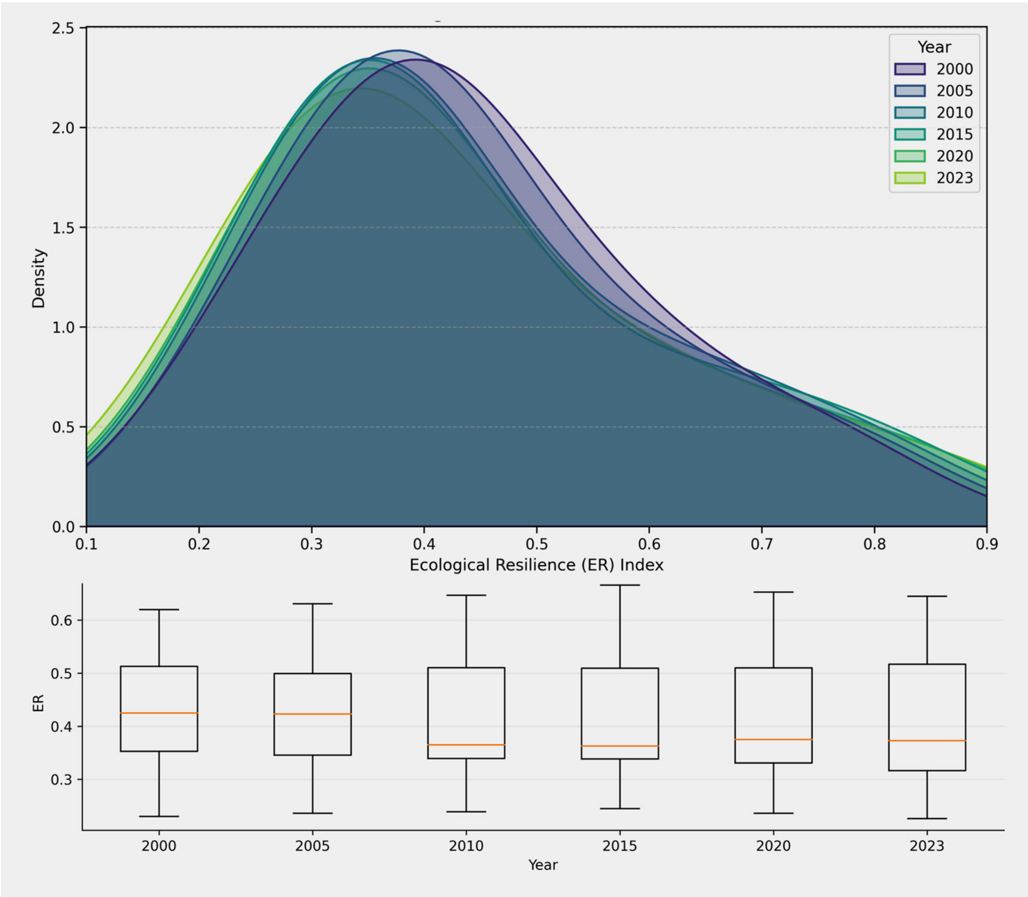

Figure 5. Temporal evolution of the distribution of the urban ecological resilience (UER) index across cities in the Guanzhong Plain Urban Agglomeration, 2000–2023.

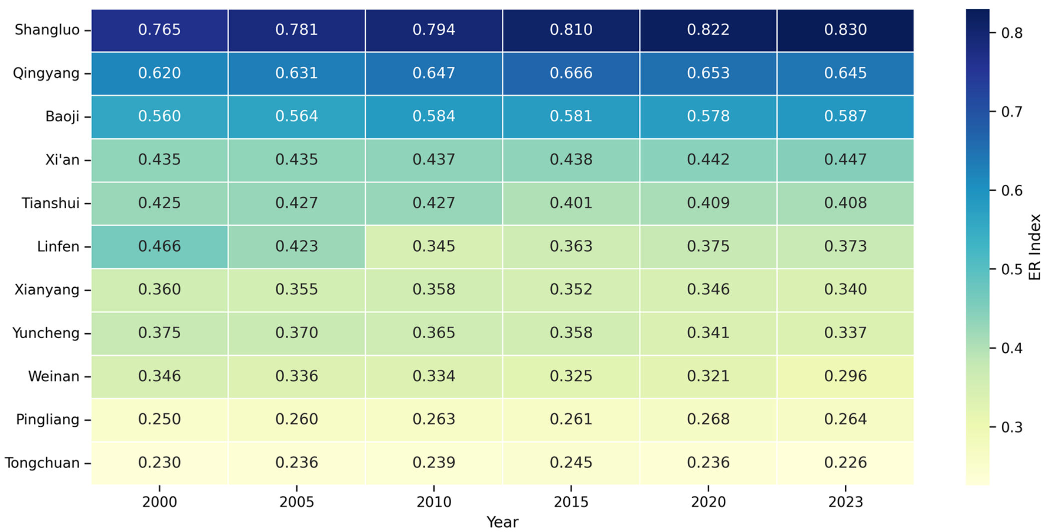

Figure 6. Spatiotemporal pattern of urban ecological resilience (UER) across cities in the Guanzhong Plain Urban Agglomeration, 2000–2023.

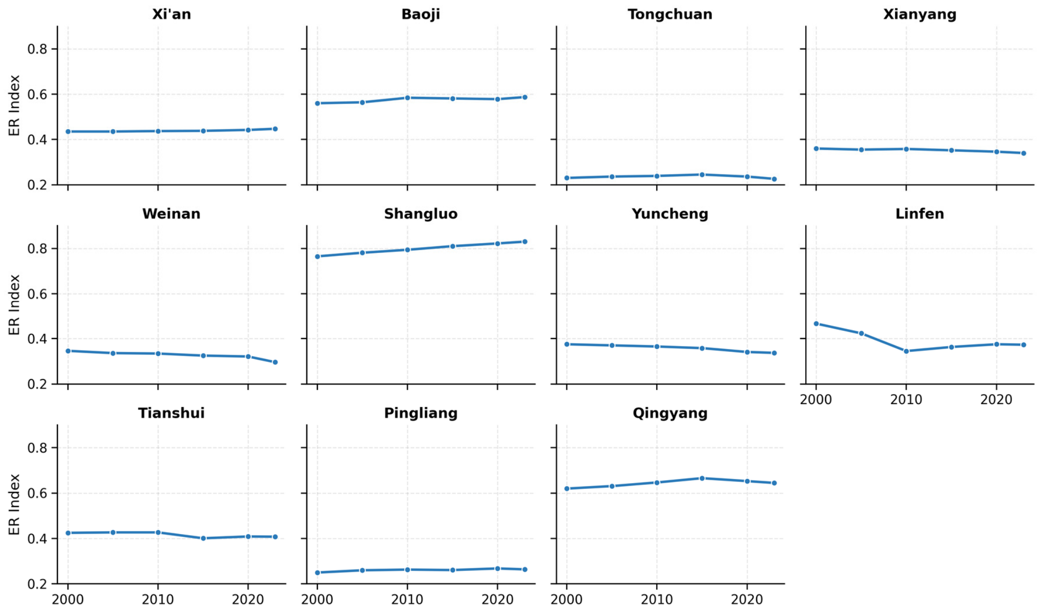

Figure 7. City-specific trajectories of urban ecological resilience (UER) in the Guanzhong Plain Urban Agglomeration, 2000–2023.

The city-specific trajectories shown in Figure 7 further illustrate pronounced heterogeneity in resilience evolution. Three broad patterns can be identified. The first is a steady accumulation pattern, characterized by relatively smooth upward trends. The second is a declining or adjustment pattern, in which resilience declines before partially recovering or stabilizing at a lower level. The third is a low-level stagnation pattern, in which UER remains persistently low with limited temporal change. Taken together, these trajectories indicate that apparent regional stability masks increasingly divergent city-level resilience pathways.

The divergent city-level trajectories can be further interpreted through three local mechanism channels. First, environmental endowment shapes the baseline level of resilience. Cities with stronger ecological buffers, higher vegetation coverage, or closer links to mountain and watershed ecological systems are more likely to maintain relatively stable resistance and recovery capacity, whereas cities located in semi-arid or loess landscapes face stronger constraints from water scarcity, soil erosion risk, and landscape fragility. Second, industrial structure affects the pressure side of resilience formation. Cities with higher dependence on energy-intensive industries or construction-driven expansion are more likely to experience declining or adjustment-type trajectories, because energy use, land conversion, and pollution pressure weaken the ecological functions underlying UER. Third, local governance and public-service capacity influence whether cities can transform development pressure into resilience gains. Cities with stronger fiscal targeting, human capital accumulation, environmental infrastructure, and ecological restoration capacity are more likely to follow steady accumulation trajectories, while cities with weaker governance capacity or limited absorptive conditions may remain in low-level stagnation. Therefore, the three trajectory types should be understood not only as statistical patterns, but also as outcomes of the interaction among ecological endowment, industrial pressure, and local governance capacity.

3.2. From Static Averages to Regime Shifts: Temporal Heterogeneity in Resilience Drivers

3.2.1. Machine-Learning Screening Identifies a Parsimonious and Robust Driver Set

Table 7 reports the robust drivers retained by Elastic Net with stability selection. Using the prespecified retention threshold, the screening procedure identifies a parsimonious set of ten drivers—FI, GDPG, HC, HCI, MHL, POP, TEC, TER, TO, and URB—which constitute the final driver set used in the subsequent post-selection estimation and heterogeneity analysis.

Table 7. Robust drivers retained by Elastic Net with stability selection, ranked by selection frequency.

Driver	Stability Selection Frequency (π)
TEC	0.945
HC	0.935
GDPG	0.880
TO	0.865
FI	0.815
TER	0.810
POP	0.800
HCI	0.775
MHL	0.750
URB	0.685

Notes: Selection frequency (π) denotes the proportion of subsampling runs in which a driver is selected with a non-zero coefficient in the Elastic Net model. Stability selection is implemented in B = 200 repeated subsamples runs, with 75% of observations drawn in each run. Drivers with $\pi \geq 0.60$ are retained as the robust set for subsequent post-selection estimation and period heterogeneity analysis. The threshold ($\pi \geq 0.60$) is used as a moderate baseline rule balancing inclusiveness and parsimony. Sensitivity checks using more stringent thresholds are reported in Appendix E.

The retained variables span multiple dimensions of the extended STIRPAT framework, including economic development, social development, industrial restructuring, demographic scale, and energy-related pressure. This result indicates that the key sources of within-city, over-time variation in UER are concentrated in a relatively small subset of socioeconomic, structural, and environmental indicators. At the same time, the screening outcome suggests that resilience formation is multidimensional rather than dominated by any single explanatory block.

In substantive terms, the machine-learning screening provides a transparent bridge between the high-dimensional candidate pool and the subsequent econometric analysis. Table 6 therefore serves as the definitive source for the stability-based driver ranking, while the following subsection focuses on how the elasticities of the screened drivers vary across periods.

3.2.2. Period Heterogeneity in Resilience–Driver Elasticities

To assess whether resilience–driver elasticities shifted across policy regimes, we estimate the period heterogeneity TWFE-STIRPAT model by interacting each selected driver with a post-2011 indicator. Table 8 reports the pre-2011 elasticities (β), the post-2011 shifts (δ), and the implied post-2011 elasticities ($\beta + \delta$). For ease of interpretation, the elasticities are also translated into the expected percentage change in UER associated with a 10% increase in each driver.

Overall, the results point to selective rather than universal regime shifts in resilience–driver elasticities. The most notable changes occur in total energy consumption (TEC), fiscal investment intensity (FI), medical and health level (MHL), and, to a lesser extent, human capital (HC). By contrast, GDP growth, trade openness, urbanization, tertiary industry share, population size, and industrial structure upgrading show limited evidence of statistically significant structural breaks.

TEC exhibits a statistically significant positive elasticity in the pre-2011 period ($\beta = 0.1278$, $p < 0.01$), while the post-2011 interaction term is negative and weakly significant ($\delta = -0.0789$, $p < 0.10$). The implied post-2011 elasticity remains positive but becomes substantially smaller. This pattern indicates that the marginal association between energy expansion and UER weakened after 2011.

Table 8. Estimated resilience–driver elasticities before and after the 2011 regime shift.

Driver	β (Pre-2011)	δ (Post Shift)	β (Post-2011)	+10% → ΔUER% (Pre)	+10% → ΔUER% (Post)
FI	−0.0281	0.0455 **	0.0174	−0.268	0.166
GDPG	0.0016	−0.0006	0.0010	0.015	0.010
HC	0.0125	−0.0305 *	−0.0180	0.119	−0.171
HCI	−0.0826	0.5953	0.5127	−0.784	5.008
MHL	−0.0332	0.1522 **	0.1190	−0.317	1.139
POP	0.0698	0.0854	0.1552	0.667	1.491
TEC	0.1278 ***	−0.0789 *	0.0489	1.225	0.478
TER	0.0104	−0.0933	−0.0829	0.099	−0.787
TO	−0.0051	−0.0018	−0.0069	−0.049	−0.066
URB	0.0062	−0.0022	0.0040	0.059	0.038

Notes: β reports the pre-2011 elasticity, and δ captures the post-2011 change, where Postt = 1 for t ≥ 2011. The implied post-2011 elasticity equals β + δ. "+10% → ΔUER%" reports the expected percentage change in UER associated with a 10% increase in each driver. All specifications include city and year fixed-effects, and standard errors are clustered at the city level. Significance levels: *** $p < 0.01$, ** $p < 0.05$, * $p < 0.10$. These estimates should be interpreted as conditional elasticities that describe how the driver–UER association changes across periods, rather than as causal estimates of one-way driver effects.

FI shows a weakly negative pre-2011 elasticity ($\beta = -0.0281$), but its post-2011 interaction term is significantly positive ($\delta = 0.0455,\ p < 0.05$), yielding a positive implied post-2011 elasticity. This represents a reversal in the fiscal investment–resilience relationship across the two periods and suggests that the resilience relevance of fiscal intervention became more favorable in the later stage.

MHL records the largest positive and statistically significant post-2011 shift among the significant interaction terms ($\delta = 0.1522,\ p < 0.05$). Its elasticity changes from negative in the pre-2011 period ($\beta = -0.0332$) to clearly positive after 2011 ($\beta + \delta = 0.1190$), indicating that the association between public health-service capacity and UER strengthened markedly in the later period.

HC shows a modest negative post-2011 adjustment ($\delta = -0.0305,\ p < 0.10$), resulting in a weaker and in some cases negative implied post-2011 elasticity despite a positive pre-2011 coefficient. By contrast, some other drivers exhibit changes in sign or magnitude but without statistically significant interaction terms, suggesting that their associations are better characterized as gradual or persistent rather than sharply regime-dependent.

These coefficient shifts should not be interpreted merely as statistical changes in elasticity. Rather, they suggest that the channels through which socioeconomic drivers affect UER changed after 2011. The weakening elasticity of TEC implies that the ecological consequences of energy expansion became less direct under stricter energy intensity control, industrial upgrading, and environmental regulation. The reversal of FI suggests that fiscal intervention increasingly shifted from growth-oriented infrastructure expansion toward ecological restoration, environmental infrastructure, and public-service provision. The strengthened role of MHL further indicates that health-service capacity became more closely connected with urban ecological resilience through improved public-service support, risk-response capacity, and ecological–health governance. Therefore, the post-2011 results provide not only evidence of temporal heterogeneity but also a mechanism-based explanation of how policy transitions reshaped the effects of key resilience drivers. These mechanisms are further discussed in Section 4.2.

To test the sensitivity of the 2011 breakpoint, we re-estimated the interaction models using 2010, 2012, 2013, and 2014 as alternative cut-off years while retaining the same stability-selected driver set. As reported in Appendix C, the main coefficient patterns remain broadly stable. FI × Post and MHL × Post are consistently positive and significant, indicating strengthened post-break roles of fiscal investment and medical-health capacity. TEC × Post remains negative across all specifications, although its significance weakens under later breakpoints, suggesting a generally weakened energy–UER association after the transition. HC × Post remains insignificant. These results indicate that the period heterogeneity findings are not driven solely by the 2011 cut-off, but reflect a broader policy regime transition.

3.3. Spatiotemporal Heterogeneity and Residual Spatial Dependence Diagnostics in Resilience Drivers

Global TWFE elasticities and regime shift estimates provide interpretable average effects, but they cannot capture the city-year non-stationarity that is likely to be important in an urban agglomeration context. We therefore employ GTWR to estimate localized and time-varying elasticities for the key retained drivers. Consistent with the empirical strategy, the local modeling focuses on four focal drivers—fiscal investment intensity (FI), human capital (HC), medical and health level (MHL), and total energy consumption (TEC)—thereby maintaining a coherent screening-to-heterogeneity framework. Residual spatial dependence is diagnosed using a row-standardized k = 3 nearest-neighbor matrix as the baseline specification, with k = 4, k = 5, and inverse-distance matrices used for robustness checks. Accordingly, spatial dependence is treated as a diagnostic and robustness issue rather than as a pre-assumed dominant mechanism.

3.3.1. City–Year Heterogeneity Revealed by GTWR

Model comparison results (Table A1) show that allowing coefficients to vary jointly over space and time substantially improves model fit relative to both global and purely spatial local specifications. Specifically, GTWR achieves the best overall performance, with $R^2 = 0.7425$, AICc $= -895.41$, and RSS $= 8.546$, outperforming OLS ($R^2 = 0.2610$, AICc $= 134.13$, RSS = 4.528) and GWR ($R^2 = 0.7098$, AICc $= -863.86$, RSS = 9.631). The GTWR output reports a cross-validation-selected optimal adaptive bandwidth of 17 nearest neighbors. Taken together, these results indicate that resilience–driver elasticities vary meaningfully across both cities and time.

The significant improvement from OLS to GWR/GTWR should be interpreted in light of the different model assumptions. OLS imposes a single global elasticity for each driver across all cities and years, whereas GTWR allows local coefficients to vary smoothly over space and time. Therefore, the increase in (R^2) reflects the presence of substantial spatiotemporal non-stationarity in the driver–UER associations. At the same time, this improvement is not interpreted as sufficient evidence of model superiority by itself. Model adequacy is evaluated jointly using AICc, RSS, in-sample fitted errors, residual normality, and residual spatial autocorrelation diagnostics.

Local coefficient summaries (Table A2) further confirm pronounced heterogeneity in the direction and magnitude of city-year local elasticities. FI exhibits a positive mean elasticity of 0.1125, but also the greatest relative dispersion (SD = 0.1222; range = −0.1289 to 0.4051; CV = 1.09), indicating strong contextual variation in the local resilience effect of fiscal intervention. HC shows a positive mean elasticity of 0.1822 with comparatively limited dispersion (SD = 0.0678; range = −0.1217 to 0.3424; CV = 0.37), suggesting a broadly stable—though not universally positive—association with UER. MHL is the only focal driver with a consistently negative mean elasticity of −0.2656, and its local coefficients lie almost entirely below zero (range = −0.4351 to −0.0112), pointing to a comparatively stable negative association across city-year contexts. TEC has a weakly negative mean elasticity of −0.0991 but high relative dispersion (SD = 0.1054; range = −0.2922 to 0.2944;

CV = 1.06), indicating that its local resilience effect varies substantially across development conditions and governance settings.

The city-year coefficient trajectories reveal distinct temporal profiles for the four focal drivers, fundamentally underscoring a "core-periphery" spatial heterogeneity within the GPUA (Figure 8). To elucidate this dynamic, we specifically highlight the evolutionary paths of two representative typologies: Xi'an (the red line), the absolute core and national central city characterized by peak factor agglomeration and a transition toward a high-tech, service-oriented economy; and Weinan (the blue line), a vital eastern gateway representing node/peripheral cities grappling with heavy-asset structures and the transition pressures of mid-to-late industrialization.

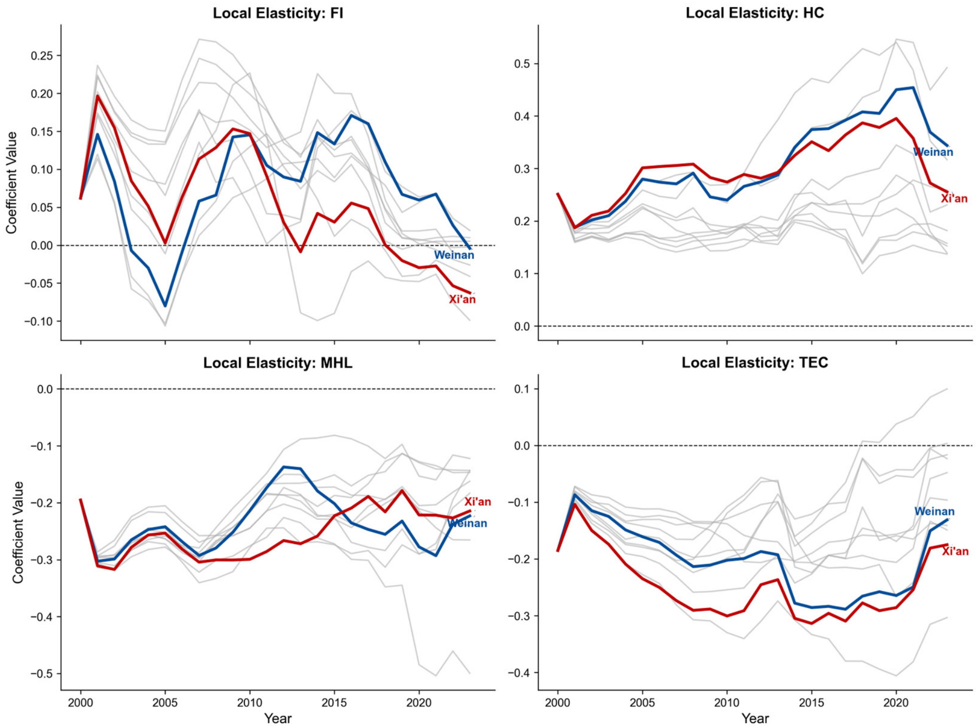

Figure 8. City-specific temporal trajectories of GTWR local coefficients for the four focal drivers in the Guanzhong Plain Urban Agglomeration, 2000–2023.

Specifically, FI follows a broadly inverted-U pattern across the region, yet the core-periphery divergence is stark. In the core city of Xi'an, the elasticity recently crossed into negative territory, indicating potential capital saturation or diminishing marginal returns, whereas it remains a positive driver in Weinan, likely reflecting the spatial spillover of capital into peripheral industrial nodes. HC, conversely, exhibits a steep, synchronized upward trajectory post-2010 for both cities, affirming that human capital accumulation has become a universal engine for UER enhancement, transcending disparate industrial structures. MHL stays predominantly negative throughout the study period, although the magnitude of this inhibitory effect generally weakens over time across all city typologies. Finally, TEC demonstrates a distinct "U-shaped" transition. While initial negative coefficients suggest early-stage technological lock-in or extensive growth penalties, the trajectories diverge sharply and trend upward after 2010. Notably, Weinan's accelerated recovery toward the zero threshold indicates that technological innovation is beginning to yield ecological resilience dividends for traditional industrial cities undergoing structural transformation. Overall, these GTWR results confirm that global-average elasticities conceal profound localized variations shaped by cities' distinct positions within the regional developmental lifecycle. The mapped local coefficients further show that this heterogeneity has a clear spatial structure, with different drivers displaying distinct city-level patterns and temporal transitions.

To further visualize the spatial disparities in local driver effects, Figure 9 maps the GTWR local coefficients of FI, HC, MHL, and TEC for 2000, 2011, and 2023. The maps reveal clear differences in both spatial distribution and temporal evolution. FI is generally positive in 2000 and becomes stronger in many central and western cities by 2011, but its positive association weakens or approaches zero in several cities by 2023. HC maintains a broadly positive spatial pattern throughout the study period, confirming its relatively stable association with UER. MHL remains negative in all three representative years, supporting its interpretation as a compound indicator of service concentration, urban pressure, and eco-health risk exposure. TEC is mainly negative, especially in southern and southeastern areas, but its local effect becomes more spatially differentiated by 2023. These spatial patterns provide intuitive evidence that resilience drivers are locally heterogeneous and temporally non-static rather than spatially uniform.

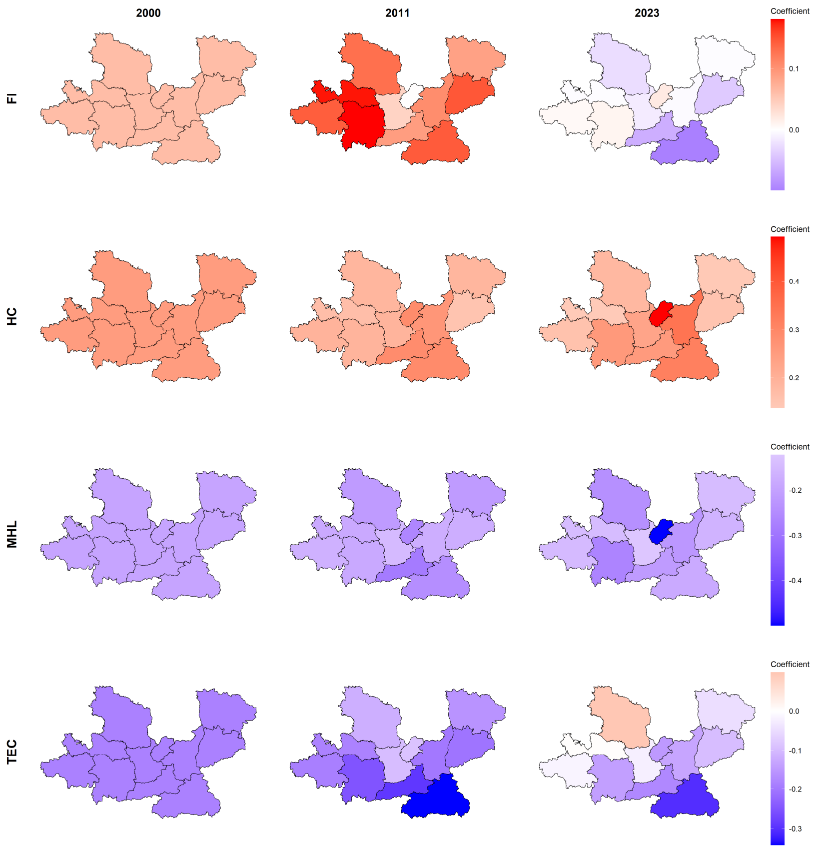

Figure 9. Spatiotemporal evolution of GTWR local coefficients for FI, HC, MHL, and TEC in the Guanzhong Plain Urban Agglomeration, 2000, 2011, and 2023. **Notes:** The three columns represent 2000, 2011, and 2023, respectively. The four rows correspond to fiscal investment intensity (FI), human capital (HC), medical and health level (MHL), and total energy consumption (TEC). Red colors indicate positive local coefficients, while blue or purple colors indicate negative local coefficients.

3.3.2. Model Validation, In-Sample Fitted Accuracy, and Residual Diagnostics

Table A3 summarizes the in-sample fitted accuracy and residual distribution diagnostics of the GTWR model. No random training−testing split is used because GTWR estimates city–year-specific local coefficient heterogeneity rather than performing out-of-sample forecasting. The reported RMSE, MAE, and MAPE are therefore calculated from fitted residuals over the full estimation sample and should be interpreted as in-sample fitted accuracy indicators. On the transformed outcome scale, GTWR shows good in-sample fitted accuracy, with RMSE = 0.1799 and MAE = 0.1448. When fitted values are back-transformed to the original UER scale, the model yields MAPE = 27.28%. These results suggest that the spatiotemporally varying specification provides a reasonable in-sample approximation to the observed resilience pattern.

Residual distributional checks indicate no strong departure from normality. As reported in Table A3, the Shapiro–Wilk test is not statistically significant (W = 0.9935, $p = 0.3040$), supporting conventional interpretation of model fit and residual behavior under the local-weighting framework. The residual mean remains close to zero (0.0313), and the overall residual spread is moderate (SD = 0.1775; range = −0.4070 to 0.4799) relative to the transformed outcome scale, further indicating that the baseline GTWR specification captures the central structure of the data reasonably well.

Residual spatial dependence was assessed using year-specific Moran's I statistics under the baseline k = 3 nearest-neighbor spatial weights matrix and three alternative specifications: k = 4, k = 5, and inverse-distance weights. The baseline k = 3 results show a mean Moran's I of −0.3026, a mean *p*-value of 0.8192, and no significant year-specific Moran's I at the 5% level (Table A4). Similar patterns are observed under the alternative weights matrices, with mean Moran's I values of −0.1754 for k = 4, −0.1503 for k = 5, and −0.1216 for the inverse-distance matrix, and no statistically significant annual tests. These results indicate that GTWR has adequately captured the main spatiotemporal structure of UER under the tested local-neighborhood and geographic distance spatial weights specifications.

The Moran's I scatterplot under the baseline k = 3 matrix shows a negative fitted slope of −0.3026, with a Pearson correlation of −0.5601 between standardized residuals and spatially lagged residuals (Figure A1). These results indicate that the GTWR residuals do not display significant positive spatial clustering. Therefore, the GTWR model appears to have adequately captured the main spatiotemporal structure of UER, with no evidence of systematic residual spatial dependence under the tested spatial weights specifications.

3.3.3. Supplementary SLM-GTWR Robustness Checks

To further assess the robustness of the GTWR-based local coefficient patterns, we estimate an SLM-GTWR specification that incorporates a spatial-lag term. This model is used as a supplementary robustness check to examine whether the main driver patterns remain stable after spatial-lag adjustment, rather than as the primary basis for identifying strong spatial spillovers.

The SLM-GTWR results are reported in Appendix A. Under the baseline (k = 3) spatial weights matrix, the model achieves (R^2 = 0.8003), adjusted (R^2 = 0.7957), AICc = −960.48, RMSE = 0.1584, MAE = 0.1252, and MAPE = 23.46% (Table A6). Alternative spatial weights specifications produce different levels of in-sample fit, with the inverse-distance matrix showing the highest fit statistics ((R^2 = 0.8976), adjusted (R^2 = 0.8952), AICc = −1136.63, and MAPE = 13.66%). This indicates that SLM-GTWR performance is sensitive to the spatial weights configuration. Therefore, the k = 3 specification is used as the baseline supplementary model because it provides a more localized neighborhood structure for the 11-city study area.

The estimated spatial-lag coefficient is negative on average under all spatial weights specifications, but its magnitude varies across matrices. Under the baseline k = 3 specification, the mean spatial-lag coefficient is −0.909, with an SD of 0.299 and a range from −1.65 to 0.0306 (Table A7). The mean values are larger in magnitude under the alternative specifications, reaching −1.97 for k = 4, −2.49 for k = 5, and −5.54 for the inverse-distance matrix. These differences indicate that the spatial-lag term is sensitive to how spatial proximity is defined. Accordingly, the spatial-lag results are interpreted as supplementary evidence of potential spatial interaction rather than as conclusive evidence of strong spatial spillovers.

Overall, the SLM-GTWR results support the robustness of the main GTWR-based interpretation. The core driver patterns remain stable after spatial-lag adjustment: HC is consistently positive, MHL remains negative but weakens after 2011, FI remains generally positive but with a weaker later-period association, and TEC remains predominantly negative. These findings reinforce the conclusion that UER drivers exhibit clear local and temporal heterogeneity, while spatial-lag effects should be interpreted cautiously as supplementary evidence rather than as the central empirical finding.

4. Discussion

Recent international literature increasingly argues that urban resilience should not be treated as a neutral, fixed, or purely technical system property. Rather, it should be understood as a relational and governance-dependent process shaped by questions of whose resilience is prioritized, which functions are protected, when and where benefits or burdens emerge, and why particular governance choices are made [58,59]. This perspective emphasizes that resilience outcomes are uneven across places, social groups, and temporal horizons, and that resilience planning often involves trade-offs among ecological protection, development needs, and governance capacities [3,58]. Building on this view, the non-static driver framework developed in this study shows that the determinants of UER should not be interpreted as fixed elasticities. Instead, they are stage-dependent and place-specific associations shaped by ecological constraints, development pathways, and governance capacity. The Discussion Section is therefore organized around three arguments: first, UER drivers are temporally non-static; second, their local associations are spatially heterogeneous; and third, resilience governance should combine stage-sensitive adjustment with place-based coordination, while recognizing cross-boundary ecological functions and environmental risks [60].

4.1. Beyond Static Drivers: Machine-Learning Screening, Structural Breaks, and Local Heterogeneity

A key contribution of this study lies in the development of an integrated analytical workflow that combines machine-learning-based variable screening with econometric structural-break testing within an extended STIRPAT framework. Although STIRPAT has been widely used to identify the drivers of environmental and sustainability outcomes, empirical applications commonly face two methodological challenges. The first is the presence of high-dimensional and highly collinear proxy variables, especially within the affluence (A) and technology (T) components. The second is the implicit assumption of temporal stationarity, whereby estimated elasticities are treated as stable across major development stages and governance transitions [8].

By combining Elastic Net regularization with stability selection, this study provides a reproducible solution to the problem of multicollinearity and model uncertainty. Unlike ad hoc variable screening or stepwise regression, which may perform poorly under correlated covariates, the stability-selection procedure identifies a parsimonious and robust set of ten drivers from an initial pool of twenty variables, while selection frequencies provide an explicit indicator of reproducibility [13,17]. This strategy reduces the likelihood that subsequent elasticity estimates are driven by redundant indicators or sample-specific noise, while preserving the policy relevance and interpretability of the STIRPAT framework [50].

As outlined in Section 2.4, the sequential design—Elastic Net screening, TWFE period interactions, GTWR local heterogeneity, and SLM-GTWR robustness testing—controls model complexity while allowing a mechanism-based interpretation of both average and local driver effects. The period heterogeneity specification shows that UER elasticities are regime-dependent rather than temporally fixed. By interacting the selected drivers with a post-2011 indicator, motivated by the transition to the 12th Five-Year Plan period and the strengthening of environmental governance, the model identifies structural shifts that would be obscured in a static specification. However, these average shifts should be interpreted together with the GTWR and baseline k = 3 SLM-GTWR results, because local models show that regime-dependent effects are not spatially uniform.

The mapped GTWR coefficients further illustrate the spatial expression of this nonstaticity. The local effects of FI, HC, MHL, and TEC display distinct city-level patterns across 2000, 2011, and 2023, indicating that regime-dependent driver relationships are filtered through local ecological constraints, development conditions, and governance contexts.

For fiscal investment intensity (FI), the period-interaction results indicate a more favorable average association after 2011, suggesting that public expenditure became increasingly linked with environmental regulation, ecological restoration, and governance capacity. The local models refine this conclusion: FI is positive on average in both GTWR and baseline k = 3 SLM-GTWR, but its magnitude varies substantially across city–year contexts and becomes weaker after 2011 in the spatial-lag robustness specification. FI should therefore be interpreted as generally beneficial but context-dependent, rather than as a uniform post-2011 improvement across all local settings.

For total energy consumption (TEC), the period-interaction results suggest an attenuation in its average marginal association after 2011, but the local models show that TEC remains predominantly negative in city–year estimates. In GTWR, TEC has a negative mean elasticity with a wide range of local values, while in the baseline (k = 3) SLM-GTWR model, it remains negative on average with very similar pre- and post-2011 means. This indicates that energy consumption continues to reflect ecological pressure in most local contexts, although its effect is increasingly conditioned by industrial structure, energy efficiency, technological upgrading, and environmental regulation.

The local results also clarify the roles of HC and MHL. Human capital (HC) is the most consistently positive driver, indicating that knowledge accumulation, skills, and adaptive capacity provide a relatively stable foundation for UER. By contrast, medical and health level (MHL) remains negative on average, although its negative association becomes weaker after 2011 in the spatial-lag robustness model. MHL should therefore not be interpreted as a purely beneficial healthcare input. Rather, it is a compound indicator associated with service concentration, urban intensity, population exposure, and eco-health risk.

Theoretically, these findings extend adaptive resilience thinking in two respects. First, they show that the contribution of a driver depends on the development stage of the urban system. Fiscal investment, for example, may be associated with ecological pressure under expansion-oriented growth, but may become more closely related to ecological restoration, environmental infrastructure, and governance capacity under a sustainability-oriented policy regime. Second, the same driver does not have equivalent meanings across places. Human capital functions as a relatively stable adaptive capacity, whereas medical-health capacity partly reflects service concentration and eco-health exposure in dense urban centers. This supports an evolutionary understanding of UER, in which resilience formation is shaped by changing institutional contexts, industrial transitions, and local absorptive capacities rather than by universal driver effects.

4.2. Policy Transmission Mechanisms Behind Post-2011 Driver Shifts

The period heterogeneity results show that the post-2011 regime shift did not affect all UER drivers uniformly. Instead, the most pronounced changes were concentrated in three dimensions: the weakened elasticity of energy consumption, the reversal of fiscal investment from a weakly negative to a positive association, and the changing role of medical-health capacity. These changes reflect not only statistical coefficient shifts, but also transformations in the policy transmission mechanisms through which socioeconomic inputs influenced UER.

First, the weakening effect of energy consumption after 2011 can be explained by the gradual decoupling between energy expansion and ecological pressure. Before 2011, energy consumption was closely associated with industrial expansion, fossil-fuel dependence, construction intensity, and pollution emissions. TEC therefore captured both the scale of resource use and the ecological disturbance generated by energy-intensive urban growth. After 2011, stricter energy intensity control, industrial restructuring, environmental regulation, and improvements in energy efficiency weakened the direct link between additional energy use and ecological degradation. The attenuated marginal association between TEC and UER suggests that the ecological relevance of energy expansion became increasingly mediated by cleaner production, technological upgrading, and regulatory constraints.

Second, the sign reversal of fiscal investment reflects a change in the functional orientation of public expenditure. Before 2011, fiscal investment in rapidly urbanizing cities was more closely related to infrastructure expansion, industrial park development, land conversion, and outward urban growth. Such growth-oriented investment could increase pressure on ecological space by accelerating construction land expansion and landscape fragmentation. After 2011, fiscal investment increasingly operated through governance-enhancing channels, including ecological restoration, environmental infrastructure, pollution control, urban greening, public-service improvement, and resilience-oriented infrastructure provision. Accordingly, FI became more favorable in the later period, suggesting that fiscal intervention was increasingly connected with ecological function maintenance and adaptive capacity enhancement.

Nevertheless, the FI coefficient should not be interpreted as a strictly causal estimate. Reverse causality may exist: cities with higher ecological resilience may be more capable of attracting or implementing fiscal investment, while cities with lower resilience may receive compensatory public investment for ecological restoration or infrastructure improvement. Thus, the FI results are best interpreted as evidence of a changing fiscal investment–resilience association and policy relevance, rather than as definitive proof of a unidirectional causal effect.

Third, the role of medical-health capacity should be understood in relation to both public-service improvement and urban pressure. Medical and health resources are not ecological variables in a narrow sense, but they reflect the capacity of urban systems to provide public services, respond to risks, and support human–environment adaptation. At the same time, higher medical-resource density is often concentrated in larger cities and regional service centers, where population concentration, land-use intensity, and environmental pressure are also higher. Therefore, the post-2011 adjustment in MHL should not be interpreted as a uniformly positive ecological effect. Instead, it indicates that the relationship between medical-health capacity and UER became less adverse and more closely connected with risk-response capacity, public-service provision, and urban adaptation. This interpretation is consistent with the local robustness results, which show that MHL remains negative in local SLM-GTWR estimates but becomes less negative after 2011.

Overall, these findings indicate that the temporal non-staticity of UER drivers is closely related to policy-induced changes in urban development pathways. The post-2011 transition reshaped the mechanisms through which fiscal investment, energy consumption, and public-service capacity affected ecological resilience: fiscal investment became more governance-oriented; the ecological sensitivity of energy consumption weakened under efficiency improvement and regulation; and medical-health capacity became less strongly associated with urban ecological pressure as public-service and risk-response functions improved.

4.3. Local Spatiotemporal Heterogeneity, City Pathways, and Spatial Weight Sensitivity

Although the TWFE-STIRPAT and period heterogeneity models provide interpretable average elasticities, they cannot fully capture the continuous spatial–temporal variation in driver effects across urban agglomerations. In the Guanzhong Plain Urban Agglomeration, resilience formation is shaped by heterogeneous ecological constraints, development trajectories, infrastructure connectivity, and governance capacity. Relying only on global-average estimates may therefore obscure important city–year differences in how socioeconomic drivers influence UER.

From this perspective, the GTWR results show that UER drivers are locally heterogeneous and temporally evolving rather than spatially uniform. The local coefficients reveal clear differences in both direction and magnitude across cities and years. The spatial coefficient maps in Figure 9 provide intuitive evidence for this heterogeneity. FI shows a stage-dependent spatial pattern, with generally positive coefficients in the early and middle stages but weaker or near-zero associations in several cities by 2023. HC maintains a broadly positive spatial pattern, confirming its relatively stable contribution to UER. MHL remains negative across representative years, supporting its interpretation as a compound indicator of service concentration, urban pressure, and eco-health risk exposure. TEC is mainly negative but becomes more spatially differentiated over time, indicating that the resilience implications of energy use depend on local industrial structure, energy efficiency, and governance capacity. Together, these patterns reinforce the conclusion that UER drivers are place-specific and temporally non-static rather than spatially uniform.

These coefficient patterns also help explain why different cities follow different resilience trajectories. Core and highly urbanized cities, such as Xi'an and Xianyang, tend to benefit disproportionately from human capital accumulation, public-service capacity, and fiscal governance resources, but they also face stronger pressures from population concentration, built-up land expansion, and service-intensive urban functions. Xi'an, as the national central city, exhibits high ecological resistance and carbon emission intensity within the agglomeration, reflecting the ecological trade-offs of concentrated urban metabolism [61].

By contrast, ecologically constrained cities in mountain, loess, or semi-arid transition zones—such as Shangluo in the Qinling Mountains, Qingyang on the Loess Plateau, and Tianshui in the Gansu mountainous corridor—are more sensitive to landscape fragmentation, water-resource stress, and land-use recovery capacity. Shangluo, as the only prefecture-level city in the GPUA entirely situated within the Qinling ecological protection zone, maintains high ecological sensitivity but low urbanization intensity, making its resistance and recovery pathways strongly dependent on natural capital endowment [62]. Qingyang, historically one of the severe soil erosion source areas in the Yellow River Basin, has undergone large-scale ecological restoration through the "Reconstructing a Ziwuling Forest" program, yet its loess landforms remain inherently fragile and its recovery capacity remains contingent on long-term vegetation cover stability.

Industrial or energy-intensive cities—including Tongchuan, Yuncheng, and Linfen—are more likely to exhibit negative or unstable TEC coefficients. Tongchuan is a nationally designated resource-exhausted city historically dominated by coal mining and cement production, while Yuncheng and Linfen have mature coal-based industrial structures. For these cities, energy use continues to represent a net ecological pressure unless accompanied by efficiency improvement, industrial upgrading, and stronger environmental regulation [22]. Thus, the observed city-level trajectories are not isolated temporal patterns, but reflect different combinations of ecological constraints, industrial structure, and governance capacity.

The residual spatial diagnostics further clarify the empirical role of spatial dependence. Using a baseline k = 3 nearest-neighbor matrix and alternative k = 4, k = 5, and inverse-distance matrices, the GTWR residuals do not show statistically significant year-specific global spatial autocorrelation. This indicates that GTWR has captured the main spatiotemporal structure of UER and that the central contribution of the spatially explicit analysis lies in identifying local coefficient heterogeneity rather than confirming strong residual spatial spillovers.

This result has an important governance implication. The absence of robust residual spatial autocorrelation does not make regional coordination unnecessary. Rather, it suggests that the primary spatial challenge in the GPUA is not a uniform spillover process, but the uneven geography of local capacities, development pressures, and ecological constraints. This interpretation is consistent with recent urban resilience literature, which argues that resilience should be understood as a relational and governance-dependent process shaped by questions of "for whom, what, when, where, and why" resilience is pursued [59]. It also aligns with critical resilience planning studies emphasizing that governance must address multi-scalar trade-offs, place-specific vulnerabilities, and differentiated institutional capacities rather than assuming that resilience benefits are evenly distributed across space [63]. Regional governance should therefore be justified not only by statistically significant spillovers, but also by shared ecological systems, infrastructure corridors, public-service networks, and environmental risks that cross administrative boundaries [60].

Within this framework, SLM-GTWR is used as a supplementary robustness specification to examine whether local driver patterns remain stable after introducing a spatial-lag term. The baseline k = 3 SLM-GTWR results show improved model fit and a negative average spatial-lag coefficient, but the magnitude of the spatial-lag coefficient varies across alternative spatial weight matrices. The spatial-lag term should therefore be interpreted cautiously as supplementary evidence of potential spatial interaction, rather than as conclusive evidence of a dominant competitive spillover mechanism.

The spillover-adjusted local coefficients further support the robustness of the main driver interpretation. HC remains the most consistently positive driver after spatial-lag adjustment, with a positive coefficient in all city–year observations. This reinforces the view that knowledge accumulation, skills, and adaptive capacity serve as durable foundations for resilience formation. Its strengthened post-2011 mean further suggests that human capital became increasingly relevant as urban ecological governance shifted toward higher-quality and more adaptive development.

The interpretation of MHL requires caution. Because MHL is measured as hospital beds per 100 persons, it captures not only healthcare capacity but also population concentration, urban intensity, and health-risk exposure. In the GPUA, higher bed density is typically observed in larger cities and regional medical centers that also face greater environmental pressure and resource demand. The negative coefficient of MHL should therefore not be read as evidence that medical resources reduce resilience. It more plausibly indicates the coupling of healthcare concentration with high-intensity urbanization, service concentration, and ecological stress. Its weaker negative association after 2011 suggests that this coupling moderated as public-service provision and ecological governance improved, although it did not disappear in local estimates.

The role of TEC also becomes clearer in the local and spatial-lag robustness results. TEC remains predominantly negative after spatial-lag adjustment, indicating that the scale of energy consumption continues to be associated with ecological pressure in most city–year contexts. However, the magnitude and direction of TEC effects vary locally, suggesting that the resilience implications of energy use depend not only on energy quantity but also on industrial structure, energy efficiency, technological upgrading, and environmental governance. This supports a transition in which resilience constraints are increasingly shaped by the quality and governance of energy use rather than by energy scale alone.

Finally, FI remains generally positive under the baseline spatial-lag robustness specification, but its local effect weakens after 2011. This suggests that fiscal investment can support UER when directed toward environmental infrastructure, ecological restoration, public services, and governance capacity. However, its effectiveness depends on policy orientation, spatial targeting, and whether investment avoids growth-oriented land expansion and inter-city competition. Thus, the resilience impact of fiscal investment depends not only on investment scale, but also on governance quality and spatial coordination.

A brief comparison with other urban agglomerations highlights the broader relevance of these findings. Studies on the Yangtze River Delta Urban Agglomeration have also reported spatially uneven ecological resilience and stage-dependent coordination between urbanization quality and ecological resilience [64]. However, compared with this more developed and humid coastal agglomeration, the GPUA represents a semi-arid and ecologically fragile urban region in the Yellow River Basin, where water scarcity, soil erosion risk, Qinling ecological protection, and energy-related industrial pressure play more central roles in shaping resilience trajectories. International metropolitan-region resilience studies likewise emphasize spatial planning, regional coordination, and differentiated local capacities [58]. The GPUA case contributes to this literature by showing that place-based governance remains important even when strong residual spatial spillovers are not statistically confirmed, because ecological functions, infrastructure networks, public services, and environmental risks cross administrative boundaries.

Overall, the empirical evidence supports two conclusions. First, UER drivers are nonstatic: their effects vary across policy stages, cities, and local development contexts. Second, the strongest evidence lies in local spatiotemporal heterogeneity rather than in strong spatial spillover effects. HC is the most robust positive driver; MHL remains negative but weakens after 2011; FI is generally positive but context-dependent; and TEC remains predominantly negative while varying across local development and governance conditions. These findings suggest that resilience governance should combine adaptive temporal policies with place-based strategies that account for local socioeconomic structures, public-service capacity, energy use patterns, and ecological governance conditions.

4.4. Policy Implications: Stage-Sensitive Targeting and Place-Based Coordination

The findings suggests that resilience governance in urban agglomerations should move beyond uniform policy prescriptions. Because resilience effects are both regime-dependent and locally heterogeneous, policy interpretation needs to combine two perspectives. On the one hand, socioeconomic drivers change their marginal effects across development stages and governance regimes. On the other hand, local resilience trajectories differ across cities because of differences in industrial structure, fiscal capacity, human capital, public-service concentration, energy use patterns, and ecological constraints. Thus, city-level resilience differences reflect not only fluctuations in the UER index, but also deeper local conditions that shape how drivers operate.

This policy orientation is consistent with recent international discussions on urban resilience governance, which argue that resilience policy should move beyond generic citywide prescriptions and instead address differentiated vulnerabilities, unequal adaptive capacities, and the institutional conditions under which resilience interventions are implemented [65]. It also responds to the knowledge–implementation gap in resilience planning, whereby technically sound frameworks must be translated into feasible governance instruments, funding mechanisms, and cross-sectoral coordination arrangements [66]. Effective resilience governance in the GPUA should therefore combine stage-sensitive policy adjustment, place-based targeting, and regional coordination where ecological functions, infrastructure networks, public services, and environmental risks cross administrative boundaries.

At the city-type level, policy priorities should be differentiated. Core urbanized cities such as Xi'an, Xianyang, Weinan, and Tongchuan should prioritize compact land-use management, green infrastructure upgrading, public-service efficiency, and the reduction in ecological pressure associated with population and service concentration. For Xi'an and Xianyang, this implies stricter green-building standards and urban growth-boundary enforcement to curb sprawl across the metropolitan corridor [62]. For Weinan and Tongchuan, compact-city strategies should be combined with industrial-park retrofitting, given their dual role as manufacturing nodes and high-carbon-emission centers [61].

Semi-arid and loess-affected cities such as Tianshui, Pingliang, and Qingyang should emphasize water-saving ecological restoration, soil erosion control, drought-resilient land management, and ecological compensation. In Qingyang, fiscal instruments should prioritize the maintenance of the Ziwuling forest restoration belt and sediment-reduction infrastructure, as its loess landforms remain inherently fragile despite decades of afforestation [67]. In Tianshui and Pingliang, ecological compensation should target watershed conservation along the Wei River tributaries, where ecological resistance differs between the Qinling foothills and urbanized valley floors [62].

Cities with strong mountain or ecological-barrier functions, especially Baoji and Shangluo, should focus on ecological corridor protection, vegetation restoration, and strict control of construction land expansion near sensitive ecological zones. Shangluo, as the only GPUA city entirely within the Qinling ecological protection zone, should enforce stricter construction land quotas and expand north–south ecological corridors connecting Qinling sources with the Wei River plain, leveraging its role as a biodiversity refuge and water-source area for the agglomeration [62]. Baoji, located at the western gateway of the Guanzhong Plain, should prioritize landscape fragmentation mitigation along expanding transport corridors [67].

Industrial or energy-pressure cities, including Yuncheng, Linfen, Weinan, and Tongchuan, should accelerate clean energy substitution, energy efficiency upgrading, and industrial decarbonization. Tongchuan, designated as a national resource-exhausted city in 2009, should leverage circular-economy industrial parks such as Dongjiahe to scale up cleaner aluminum and automotive-component manufacturing. Yuncheng and Linfen should integrate coal-industry efficiency mandates with provincial carbon-peaking targets to reduce legacy energy intensity [22]. In this way, regional resilience governance can combine a common ecological-security objective with differentiated city-level implementation priorities.

4.4.1. Human Capital: From Local Talent Accumulation to Shared Adaptive Capacity

The discussion of HC points to a broad policy implication: its resilience benefits depend less on simple talent concentration than on the capacity to translate knowledge and skills into adaptive governance, innovation, and ecological problem-solving. HC is the most consistently positive driver in both GTWR and baseline $k = 3$ SLM-GTWR estimates, indicating that human capital enhances absorptive capacity, policy learning, technical adaptation, and environmental-management capability. The stable positive spatial pattern of HC further suggests that human capital policy can serve as a cross-cutting resilience strategy across the agglomeration, although implementation should reflect local absorptive capacity.

Policy should therefore shift from city-by-city talent competition toward regional capability building. Practical measures include cross-city green-skills training, university-industry collaboration, ecological-governance knowledge platforms, and technical assistance mechanisms for cities with weaker innovation and administrative capacity. Such policies would help convert human capital advantages into shared adaptive capacity rather than allowing them to remain concentrated in a few core cities.

In the GPUA, Xi'an and Xianyang should function as regional knowledge and training hubs, leveraging their universities and research institutes to support Tianshui, Pingliang, and Qingyang, where information and migration-network centrality remains weak [68]. For Shangluo and Tongchuan, targeted capacity-building should focus on ecological monitoring, low-carbon industrial management, land-use planning, and environmental project implementation, because their intermediary communication with core cities depends on stronger institutional linkages [68].

4.4.2. Medical and Health Capacity: From Service Concentration to Eco-Health Risk Governance

The policy meaning of MHL requires a broader interpretation. Since MHL is measured by hospital beds per 100 persons, it captures not only healthcare provision but also population concentration, urban intensity, and potential health-risk exposure. The empirical results show that MHL remains negatively associated with UER in local estimates, although this negative association weakens after 2011. Thus, MHL should not be interpreted as evidence that medical resources reduce ecological resilience. It more plausibly reflects the coupling of service concentration, urban pressure, and eco-health risk exposure.

Policy should therefore avoid relying solely on the expansion of medical facilities in already concentrated urban centers. What matters is reducing the ecological and public-health stress that makes such concentration necessary. This requires a shift from reactive service expansion toward preventive eco-health governance, in which environmental remediation, pollution control, public-health preparedness, green infrastructure, and climate-risk adaptation are treated as part of the same resilience agenda.

In the GPUA, this eco-health governance scale should be organized around the Fen–Wei River basin axis, where Xi'an, Xianyang, and Weinan share contiguous air-pollution exposure and water-quality degradation gradients [61]. Joint monitoring of air pollution, heat exposure, and environmental-health risks should therefore cover this central corridor as a single epidemiological unit. Peripheral cities such as Shangluo and Qingyang should be integrated into regional medical-response networks rather than duplicating bed-capacity expansion that their smaller populations cannot sustain efficiently. For high-pressure cities, medical-resource planning should be integrated with pollution reduction, ecological restoration, compact urban management, and health-risk prevention.

4.4.3. Energy Consumption: From Scale Control to Structural and Efficiency-Oriented Transition

The discussion of TEC suggests that resilience constraints are shaped not only by how much energy is consumed, but also by how energy use is embedded in industrial structure, technological efficiency, and environmental governance. The period-interaction results indicate that the average marginal association of TEC with UER becomes attenuated after 2011, while GTWR and baseline k = 3 SLM-GTWR results show that TEC remains predominantly negative in many city–year contexts. Energy consumption therefore continues to reflect ecological pressure, but its resilience implication is increasingly conditioned by energy efficiency, industrial upgrading, cleaner production, and regulatory capacity.

Energy policy should move beyond simple quantitative restraint. A more effective direction is a coordinated structural transition centered on clean energy substitution, efficiency upgrading, industrial decarbonization, and harmonized environmental standards. For urban agglomerations, energy adjustment should also consider industrial-chain linkages and infrastructure systems, so that emission reduction and energy efficiency improvements do not merely shift ecological pressure across jurisdictions.

Cities with stronger negative TEC coefficients should prioritize clean energy replacement, industrial decarbonization, and strict energy efficiency improvement, while cities with weaker negative associations should consolidate efficiency gains and prevent the relocation or rebound of energy-intensive activities. In the GPUA, Tongchuan and Weinan, where carbon emission cores are concentrated due to coal-to-aluminum and energy-chemical industries, should be prioritized for industrial-park retrofitting and clean-energy substitution [61]. Yuncheng and Linfen, as mature coal cities in the Shanxi section of the agglomeration, should be subject to cross-provincial harmonized environmental standards to prevent emission leakage across jurisdictions [22]. For Xi'an and Xianyang, where TEC coefficients approach weaker negative effects in later years, policy should prevent the rebound of energy-intensive service activities and ensure that green infrastructure keeps pace with population concentration.

4.4.4. Fiscal Investment: From Expenditure Expansion to Targeted Ecological Governance

The interpretation of FI should also be refined. The period heterogeneity results suggest that its average effect becomes more favorable after 2011, while GTWR and baseline $k = 3$ SLM-GTWR results show that FI remains generally positive but locally heterogeneous. In the spatial-lag robustness specification, FI is still positive on average, but its post-2011 mean is lower than its pre-2011 mean. This indicates that fiscal resources can support UER, but their effectiveness depends on governance orientation, spatial targeting, and implementation quality rather than expenditure scale alone.

Policy should therefore move from scale-oriented fiscal expansion toward targeted and performance-based ecological governance. Fiscal instruments such as ecological compensation, cross-boundary environmental funds, watershed and corridor restoration projects, public-service equalization mechanisms, and shared appraisal systems can help ensure that public investment supports resilience formation rather than fragmented local expansion. In the GPUA, fiscal investment should be evaluated not only by expenditure scale, but also by ecological performance, spatial targeting, and coordination across administrative boundaries.

For example, the Wei River and Qinling ecological corridor, spanning Xi'an, Xianyang, Baoji, and Shangluo, requires a basin-level fiscal-pooling mechanism rather than separate city-level green budgets, because ecological sources and corridors are concentrated in the south while ecological breakpoints are concentrated in the central plain [62]. Similarly, Qingyang's sediment-reduction infrastructure and Tianshui's watershed conservation should be eligible for cross-provincial ecological compensation from downstream beneficiaries in the Shaanxi plain, because their upstream conservation services generate positive externalities for the entire agglomeration [67].

Overall, the policy implications point to a stage-sensitive and place-based governance strategy. Human capital should be translated into shared adaptive capacity; medical-health capacity should be integrated into preventive eco-health governance; energy policy should emphasize structural and efficiency-oriented transition; and fiscal investment should be redirected toward targeted ecological governance. These policy directions correspond to the empirical finding that UER drivers are non-static, locally heterogeneous, and conditioned by both development stage and governance context. In practical terms, resilience governance in the GPUA should combine common regional objectives with differentiated city-level priorities, so that interventions match the spatially heterogeneous driver patterns revealed by the GTWR coefficient maps.

5. Conclusions

This study explained how urban ecological resilience (UER) is formed and what drives it in the Guanzhong Plain Urban Agglomeration under rapid urbanization and tightening ecological constraints. By combining three-dimensional resilience measurement, Elastic Net-based driver screening, structural-break analysis, GTWR-based local modeling, and supplementary SLM-GTWR robustness checks, the study shows that UER drivers are dynamic rather than fixed, and that resilience formation is shaped mainly by governance-regime shifts and localized heterogeneity. The framework addresses two recurring limitations in the existing literature: unstable variable selection under multicollinearity and the assumption of temporally fixed elasticities. It also provides a cautious spatial diagnostic framework, in which spatial-lag results are interpreted as supplementary evidence because they are sensitive to spatial weight specifications.

Three main conclusions can be drawn. First, UER in the GPUA shows relative stability at the regional aggregate level but increasing divergence across cities, indicating that resilience formation is not a uniform regional process but is shaped by uneven local development pathways. Second, resilience drivers are temporally non-static. Machine-learning screening identifies a parsimonious and robust set of key drivers, while period heterogeneity analysis shows that their elasticities shift across governance stages. Third, GTWR reveals marked city–year heterogeneity in local driver associations. Residual Moran's I diagnostics based on k-nearest-neighbor and inverse-distance weights show no robust evidence of remaining global spatial autocorrelation after GTWR, while SLM-GTWR results suggest that the main local coefficient patterns remain generally stable after spatial-lag adjustment. Therefore, the spatial-lag term should be treated as supplementary rather than central evidence.

These findings carry both methodological and substantive implications. Methodologically, the study shows that resilience analysis benefits from moving beyond static average-effect models toward an integrated framework that combines machine-learning screening, regime-sensitive econometric analysis, GTWR-based local heterogeneity analysis, residual spatial diagnostics, and supplementary spatial-lag robustness checks. Substantively, the results suggest that resilience governance in urban agglomerations should not rely on uniform policy prescriptions. Instead, it should combine place-based targeting, because driver associations vary across cities and development stages, with regional coordination, because ecological functions, infrastructure networks, public services, and environmental risks often cross administrative boundaries, even when strong residual spatial spillovers are not statistically confirmed. In mature development stages, strengthening human capital, ecological governance capacity, public-service coordination, and energy efficiency improvement appears more effective than continued reliance on resource- and construction-intensive expansion.

Despite its dynamic and spatially explicit design, this study has several limitations. First, the spatial robustness checks are based mainly on local-neighborhood and geographic distance assumptions. Although alternative k-nearest-neighbor and inverse-distance matrices were compared, other forms of spatial connectivity, such as economic linkages, transport networks, functional flows, or administrative contiguity, were not fully examined. Second, the analysis was conducted at the prefecture level, which is appropriate for long-term socioeconomic panel modeling but may not fully capture ecological process boundaries, including watersheds, mountain systems, ecological corridors, soil-erosion zones, and climate-sensitive transition belts. Third, climatic factors were not directly incorporated into the empirical models, although precipitation, temperature, drought intensity, evapotranspiration, and extreme climate events may substantially affect ecological resilience in semi-arid urban agglomerations. In addition, some measurement components rely on literature-based coefficients and interpolation of isolated missing values, which may introduce uncertainty into the resilience index and smooth short-term fluctuations. Finally, the empirical framework identifies non-static associations and local heterogeneity rather than strict causal effects.

Future research could extend this study in several directions. First, broader spatial weight specifications and larger multi-region samples could be used to examine whether the observed local heterogeneity remains stable under different assumptions about inter-city relationships. Second, future studies could adopt watershed-based, grid-based, or multi-scale spatial units to better align empirical analysis with ecological processes and within-city heterogeneity. Third, integrating climatic datasets with land-use, ecosystem service, and socioeconomic indicators would help clarify climate–ecosystem–urbanization interactions in environmentally constrained regions. Fourth, the measurement of UER could be strengthened through locally calibrated ecosystem service models, restoration monitoring data, field observations, expert elicitation, and sensitivity tests using alternative coefficient schemes and missing-data treatments. Finally, future work could incorporate instrumental variables, quasi-natural experiments, dynamic panel models, or policy-based causal designs to strengthen causal inference. Overall, the integrated framework developed in this study provides a transferable basis for understanding resilience formation in environmentally constrained urban agglomerations and for supporting adaptive, place-based, and regionally coordinated sustainability governance.

Author Contributions: Conceptualization, Y.W. and X.D.; Software, Y.W. and K.L.; Validation, R.L. and K.L.; Formal analysis, Y.W. and R.L.; Investigation, Y.W. and H.W.; Resources, X.D. and H.W.; Data curation, K.L. and R.L.; Writing—original draft preparation, Y.W.; Writing—review and editing, X.D., H.W. and R.L.; Visualization, K.L. and H.W.; Supervision, X.D. and H.W.; Project administration, X.D. and H.W.; Funding acquisition, X.D. All authors have read and agreed to the published version of the manuscript.

Funding: This research was funded by the "National Office for Philosophy and Social Sciences (22BGL195)".

Data Availability Statement: The raw data supporting the conclusions of this article will be made available by the authors on request.

Conflicts of Interest: The authors declare no conflicts of interest.

Abbreviations

UER	Urban Ecological Resilience
GPUA	Guanzhong Plain Urban Agglomeration
STIRPAT	Stochastic Impacts by Regression on Population, Affluence, and Technology
TWFE	Two-way Fixed-Effects
EN	Elastic Net
GTWR	Geographically and Temporally Weighted Regression
GWR	Geographically Weighted Regression
SLM-GTWR	Spatial Lag Geographically and Temporally Weighted Regression
OLS	Ordinary Least Squares
LULC	Land-Use/Land-Cover
ESV	Ecosystem Service Value
SHDI	Shannon's Diversity Index
AWMPFD	Area-weighted Mean Patch Fractal Dimension

PD_L	Patch Density, landscape metric
FI	Fiscal Investment Intensity
GDPG	GDP Growth Rate
PGDP	GDP per Capita
HC	Human Capital Level
HCI	Industrial Structure Upgrading Index
MHL	Medical and Health Level
POP	Population Size
PD	Population Density
TEC	Total Energy Consumption
PCEC	Per Capita Energy Consumption
EI	Energy Intensity
CEI	Carbon Emissions per Unit Energy Consumption
CDE	Carbon Dioxide Emissions
TER	Contribution Rate of Tertiary Industry to GDP
TO	Trade Openness
URB	Urbanization Level
PRI	Contribution Rate of Primary Industry to GDP
SEC	Contribution Rate of Secondary Industry to GDP
ISA	Industrial Structure Advancement
EDU	Education Expenditure Level
RSS	Residual Sum of Squares
AICc	Corrected Akaike Information Criterion
RMSE	Root Mean Squared Error
MAE	Mean Absolute Error
MAPE	Mean Absolute Percentage Error
CV	Coefficient of Variation
VIF	Variance Inflation Factor
KDE	Kernel Density Estimation
CNY	Chinese Yuan
tce	Tons of Coal Equivalent

Appendix A. Supplementary Data and Tables

This appendix reports supplementary model comparison results, GTWR local coefficient summaries, predictive diagnostics, residual spatial autocorrelation tests, and supplementary SLM-GTWR robustness results. GTWR residual spatial dependence is evaluated using a baseline row-standardized k = 3 nearest-neighbor spatial weights matrix, with k = 4, k = 5, and inverse-distance matrices used for robustness checks. SLM-GTWR is reported as a supplementary spatial-lag robustness specification rather than as the primary model for identifying spatial spillovers.

Table A1. Comparative performance of global, spatial, and spatiotemporal specifications for urban ecological resilience.

Model	Bandwidth/Kernel	R^2	AICc	RSS
OLS	Global	0.2610	134.13	24.528
GWR	Adaptive Gaussian spatial kernel	0.7098	−863.86	9.631
GTWR	Adaptive Gaussian spatiotemporal kernel; CV-selected optimal bandwidth = 17 nearest neighbors	0.7425	−895.41	8.546

Notes: The GTWR bandwidth is selected using a cross-validation-based criterion and refers to the adaptive spatiotemporal kernel used for local coefficient estimation. AICc is reported as a post-estimation model comparison indicator and is not used as the GTWR bandwidth-selection criterion. The GTWR bandwidth is different from the k-nearest-neighbor spatial weights matrices used for Moran's I residual diagnostics.

Table A2. Summary statistics of city-year local coefficients from the GTWR model.

Driver	Mean	SD	Min	Max	CV
FI	0.1125	0.1222	−0.1289	0.4051	1.09
HC	0.1822	0.0678	−0.1217	0.3424	0.37
MHL	−0.2656	0.0775	−0.4351	−0.0112	0.29
TEC	−0.0991	0.1054	−0.2922	0.2944	1.06

Notes: This table summarizes the empirical distribution of city–year local coefficients estimated by the GTWR model for the four focal drivers. All drivers are log-transformed and standardized before estimation; therefore, the coefficients should be interpreted as standardized local associations rather than raw marginal effects. "Mean", "SD", "Min", and "Max" report the central tendency and dispersion of the local coefficient estimates across all city–year observations. CV denotes the coefficient of variation, calculated as **SD**/ | **Mean** |, and is used as a scale-free indicator of relative heterogeneity. When the mean coefficient is close to zero, the CV should be interpreted together with the SD and min–max range. Positive mean coefficients indicate a generally positive association with UER, whereas negative mean coefficients indicate a generally negative association.

Table A3. In-sample fitted accuracy and residual distribution diagnostics of the GTWR model.

Panel	Metric	Value
A. In-sample fitted accuracy	Number of observations (N)	264
	RMSE (log-transformed outcome scale)	0.1799
	MAE (log-transformed outcome scale)	0.1448
	MAPE (back-transformed UER scale, %)	27.28
B. Residual distribution	Mean residual	0.0313
	Median residual	0.0167
	Standard deviation of residuals	0.1775
	Minimum residual	−0.407
	Maximum residual	0.4799
C. Normality check	Shapiro–Wilk W	0.9935
	Shapiro–Wilk *p*-value	0.304

Notes: Panel A reports in-sample fitted accuracy of the GTWR model. RMSE and MAE are computed on the log-transformed and standardized outcome scale, whereas MAPE is calculated on the back-transformed UER scale. These metrics are calculated using fitted residuals from the full estimation sample and should not be interpreted as independent test-set prediction errors. Panel B summarizes the empirical distribution of GTWR residuals, and Panel C reports the Shapiro–Wilk normality test. Lower RMSE, MAE, and MAPE indicate better predictive performance.

Table A4. Sensitivity of year-specific Moran's I diagnostics for GTWR residuals under alternative spatial weights matrices.

Weight	Role	Matrix	k	Mean I	SD	Range	Mean *p*	Sig. Years
k = 3	Baseline	k-NN	3	−0.3026	0.1242	−0.5080 to −0.1328	0.8192	0%
k = 4	Robustness	k-NN	4	−0.1754	0.0697	−0.3083 to −0.0145	0.6912	0%
k = 5	Robustness	k-NN	5	−0.1503	0.0387	−0.2298 to −0.0850	0.6640	0%
Inverse-distance	Robustness	Inverse-distance	—	−0.1216	0.0318	−0.1747 to −0.0642	0.6290	0%

Notes: Residual Moran's (I) statistics are calculated annually using GTWR residuals and summarized across 2000–2023. The baseline spatial weights matrix is row-standardized (k = 3) nearest neighbors. Robustness checks are conducted using (k = 4), (k = 5), and inverse-distance weights. Across all four specifications, no year-specific Moran's (I) statistic is significant at the 5% level.

Table A5. Year-specific Moran's I diagnostics for GTWR residuals under the baseline k = 3 spatial weights matrix.

Year	N Cities	Moran's I	Expected I	Variance	*p*-Value	Significant at 5%
2000	11	−0.1807	−0.1000	0.0350	0.6669	No
2001	11	−0.2313	−0.1000	0.0348	0.7595	No
2002	11	−0.2438	−0.1000	0.0315	0.7910	No
2003	11	−0.2853	−0.1000	0.0325	0.8479	No

Table A5. *Cont.*

Year	N Cities	Moran's I	Expected I	Variance	*p*-Value	Significant at 5%
2004	11	−0.5080	−0.1000	0.0309	0.9899	No
2005	11	−0.4598	−0.1000	0.0350	0.9728	No
2006	11	−0.4971	−0.1000	0.0349	0.9833	No
2007	11	−0.4996	−0.1000	0.0316	0.9878	No
2008	11	−0.4700	−0.1000	0.0344	0.9769	No
2009	11	−0.3177	−0.1000	0.0361	0.8740	No
2010	11	−0.2557	−0.1000	0.0306	0.8132	No
2011	11	−0.3100	−0.1000	0.0338	0.8733	No
2012	11	−0.3988	−0.1000	0.0328	0.9504	No
2013	11	−0.1841	−0.1000	0.0305	0.6849	No
2014	11	−0.2768	−0.1000	0.0347	0.8288	No
2015	11	−0.1619	−0.1000	0.0342	0.6311	No
2016	11	−0.1568	−0.1000	0.0348	0.6196	No
2017	11	−0.1328	−0.1000	0.0330	0.5717	No
2018	11	−0.3299	−0.1000	0.0349	0.8908	No
2019	11	−0.1683	−0.1000	0.0307	0.6515	No
2020	11	−0.3976	−0.1000	0.0343	0.9460	No
2021	11	−0.4065	−0.1000	0.0346	0.9503	No
2022	11	−0.2209	−0.1000	0.0318	0.7513	No
2023	11	−0.1698	−0.1000	0.0342	0.6472	No

Notes: This table reports year-specific residual spatial autocorrelation diagnostics under the baseline row-standardized k = 3 nearest-neighbor matrix. None of the annual Moran's I statistics is significant at the 5% level.

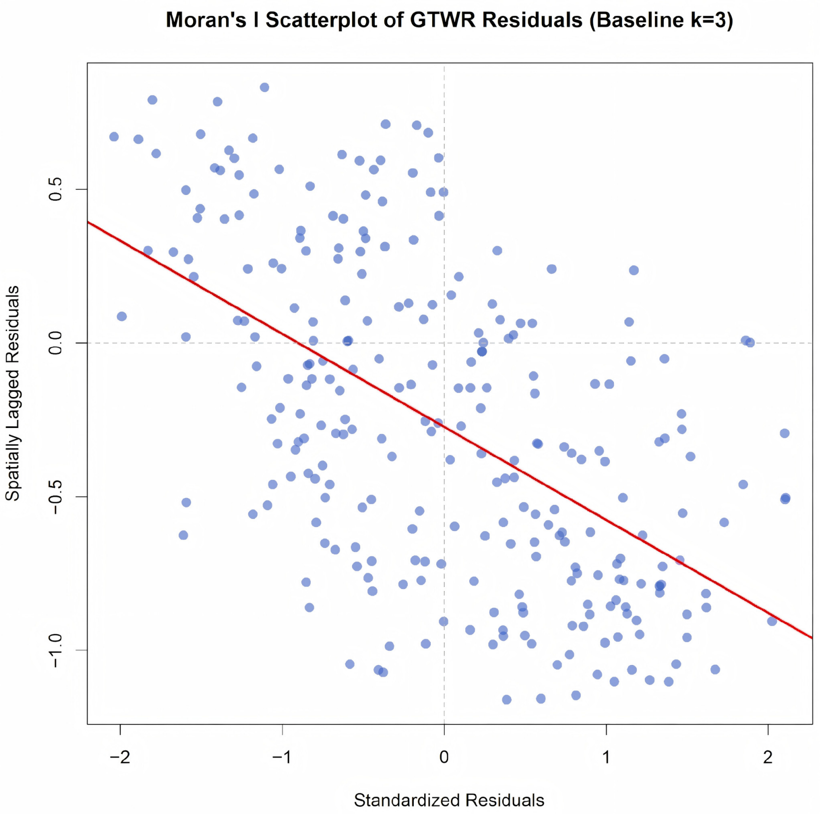

Figure A1. Moran's I scatterplot of GTWR residuals under the baseline k = 3 spatial weights matrix. **Notes:** The fitted red line has a slope of −0.3026, corresponding to the Moran-scatter slope under the baseline k = 3 matrix. The Pearson correlation between standardized residuals and spatially lagged residuals is −0.5601. The negative slope and non-significant year-specific Moran's I diagnostics indicate no significant positive residual spatial clustering under the baseline local-neighborhood specification.

Table A6. Model fit and predictive accuracy of the SLM-GTWR under alternative spatial weights.

Weight Spec	Role	Matrix Type	k	R^2	Adj. R^2	AICc	RMSE	MAE	MAPE (%)
k = 3	Baseline	k-nearest neighbors	3	0.8003	0.7957	−960.4831	0.1584	0.1252	23.46
k = 4	Robustness	k-nearest neighbors	4	0.8572	0.8538	−1048.8843	0.1340	0.1105	17.15
k = 5	Robustness	k-nearest neighbors	5	0.8440	0.8403	−1025.5502	0.1401	0.1139	18.36
Inverse-distance	Robustness	inverse-distance	-	0.8976	0.8952	−1136.6294	0.1135	0.0922	13.66

Notes: This table reports goodness-of-fit and predictive accuracy metrics for the supplementary SLM-GTWR specification. The baseline model uses a row-standardized k = 3 nearest-neighbor spatial weights matrix. Robustness checks are conducted using k = 4, k = 5, and inverse-distance matrices. The differences across specifications indicate that SLM-GTWR fit statistics are sensitive to the choice of spatial weights matrix.

Table A7. Summary of the spatial-lag coefficient (Rho) from the SLM-GTWR model.

Weight Spec	Role	Matrix Type	k	Mean	SD	Min	Max
k = 3	Baseline	k-nearest neighbors	3	−0.909	0.299	−1.65	0.0306
k = 4	Robustness	k-nearest neighbors	4	−1.97	0.654	−3.45	−0.384
k = 5	Robustness	k-nearest neighbors	5	−2.49	0.594	−3.94	−0.906
Inverse-distance	Robustness	inverse-distance	—	−5.54	1.08	−8.26	−3.79

Notes: This table summarizes the distribution of the spatial-lag coefficient (\rho) in the supplementary SLM-GTWR model. The spatial-lag coefficient captures the association between local UER and the spatially lagged UER term under each spatial weights specification. Because the magnitude of (\rho) varies considerably across weights matrices, it should be interpreted as supplementary evidence of potential spatial interaction rather than as conclusive evidence of strong spatial spillovers.

Table A8. Spatial-lag-adjusted local coefficients for focal drivers under the baseline k = 3 SLM-GTWR model.

Variable	Mean	SD	Min	Max	Positive Share (%)	Pre-2011 Mean	Post-2011 Mean
FI	0.0792	0.0812	−0.1065	0.2713	82.58	0.1084	0.0544
HC	0.2403	0.0892	0.0995	0.5461	100	0.2078	0.2677
MHL	−0.2354	0.0648	−0.5039	−0.0815	0	−0.2638	−0.2114
TEC	−0.1683	0.0832	−0.4058	0.0996	2.65	−0.1658	−0.1704

Notes: This table reports local coefficient estimates for the focal drivers after including the spatial-lag term in the baseline k = 3 SLM-GTWR model. "Positive share" denotes the proportion of city–year observations with positive local coefficients. "Pre-2011 mean" and "Post-2011 mean" report the average local coefficients before and after 2011. The results are used as a supplementary robustness check for the GTWR-based local coefficient patterns.

Table A9. Pooled Moran's I diagnostics for SLM-GTWR residuals.

Weight Spec	Scope	N Obs	Moran's I	Expected I	*p*-Value (Permutation)	Significant (5%)
k = 3	Pooled_city_year	264	−0.0871	−0.0980	0.803	FALSE
k = 4	Pooled_city_year	264	0.0249	−0.0984	0.001	TRUE
k = 5	Pooled_city_year	264	−0.0640	−0.0988	0.135	FALSE
Inverse-distance	Pooled_city_year	264	−0.0624	−0.0996	0.004	TRUE

Notes: This table reports pooled residual spatial autocorrelation diagnostics for the supplementary SLM-GTWR model across all 264 city–year observations using permutation-based inference. Under the baseline k = 3 specification, the pooled residual Moran's I is not statistically significant. The k = 4 and inverse-distance specifications produce significant pooled Moran's I, indicating that residual diagnostics are sensitive to the definition of spatial weights. Therefore, the SLM-GTWR results are interpreted as supplementary robustness evidence, with the baseline k = 3 specification retained for its local-neighborhood interpretation in the 11-city study area.

Appendix B. Robustness Check of the UER Index Under Alternative Adaptability Weighting

To examine whether the composite UER index is sensitive to weighting assumptions in the indicator construction process, we conducted an additional robustness test by modifying the internal weights of the adaptability dimension. In the baseline index, the adaptability dimension is constructed from two components: landscape heterogeneity and landscape fragmentation/connectivity. SHDI and AWMPFD are used to characterize landscape heterogeneity, each with a weight of 0.25, while reverse-coded PD is used to characterize fragmentation/connectivity, with a weight of 0.50. This setting reflects the view that landscape heterogeneity and connectivity represent two core but non-substitutable aspects of ecological structural stability.

As a sensitivity test, we assigned equal weights to the three landscape metrics, namely SHDI, AWMPFD, and reverse-coded PD, with each receiving a weight of one-third. The adaptability index and the composite UER index were then recalculated using the alternative weighting scheme (Figures A2 and A3). The results show that the revised adaptability index exhibits a slightly lower overall level, but its temporal trend remains consistent with the baseline index. In addition, the reconstructed UER index is highly consistent with the original UER index, with no substantial changes in interannual fluctuations, key turning points, or overall temporal patterns.

These findings indicate that the baseline UER index is not materially driven by the specific internal weighting scheme of the adaptability dimension. Although the choice of weights affects the absolute value of the adaptability sub-index, it does not change the main spatiotemporal pattern of UER or the subsequent empirical conclusions. Therefore, the baseline weighting scheme is considered robust and is retained in the main analysis.

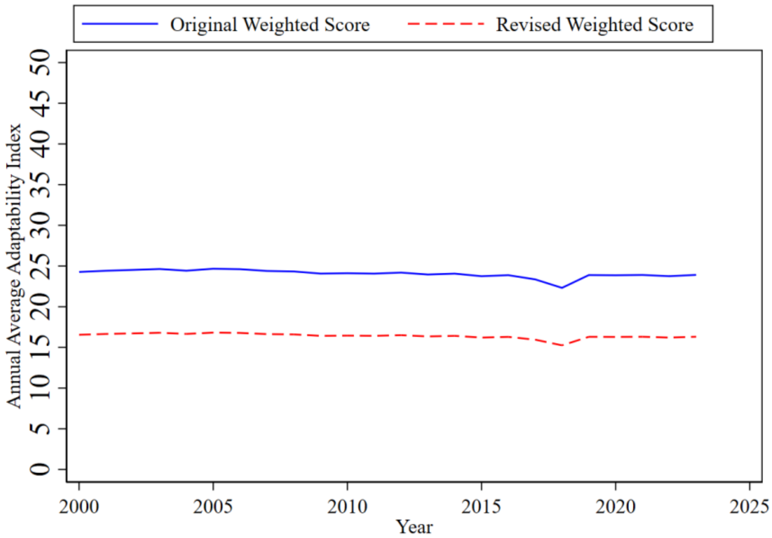

Figure A2. Sensitivity of the adaptability index to alternative metric weighting schemes.

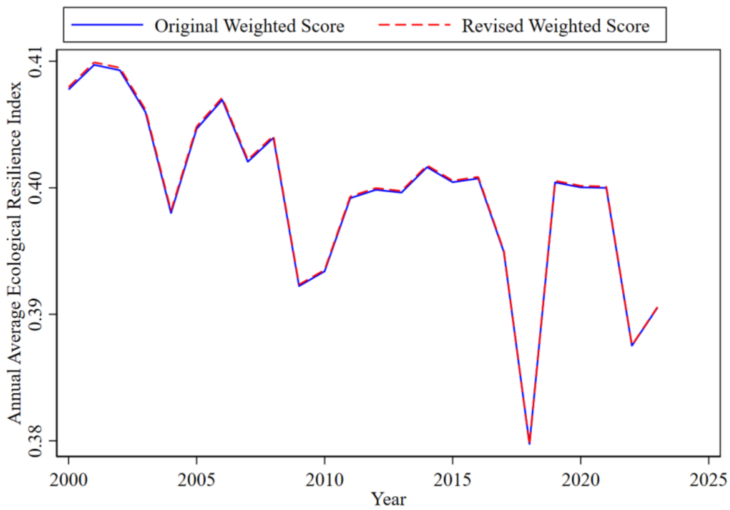

Figure A3. Comparison of the composite UER index under baseline and alternative adaptability weighting schemes.

Appendix C. Alternative Breakpoint Robustness Check for TWFE-STIRPAT Period Heterogeneity

Appendix C reports robustness checks using alternative breakpoint years around the 2011 baseline transition. Specifically, the period-interaction TWFE models were re-estimated using 2010, 2012, 2013, and 2014 as alternative breakpoints, while keeping the same stability-selected driver set across all specifications. The comparison shows that the main coefficient patterns are broadly robust (Table A7). FI × Post remains positive and statistically significant under all breakpoint specifications, and MHL × Post also remains positive and significant. TEC × Post remains negative across all specifications, although its statistical significance weakens under later breakpoints. HC × Post remains statistically insignificant. Overall, these results support the interpretation that the observed period heterogeneity reflects a broader policy regime transition rather than an artifact of the specific 2011 cut-off.

Table A10. Robustness of period heterogeneity results under alternative breakpoint years.

Driver	2010	2011 Baseline	2012	2013	2014	Interpretation
TEC × Post	−0.0341 *** (0.001)	−0.0301 *** (0.007)	−0.0263 ** (0.049)	−0.0233 (0.126)	−0.0211 (0.219)	Negative direction remains stable; significance weakens under later breakpoints
FI × Post	0.0579 *** (0.001)	0.0478 *** (0.001)	0.0404 *** (0.003)	0.0353 ** (0.014)	0.0317 ** (0.045)	Positive and significant across all breakpoint specifications
MHL × Post	0.0698 ** (0.023)	0.0881 *** (0.009)	0.1040 ** (0.011)	0.1118 ** (0.019)	0.1149 ** (0.036)	Positive and significant across all breakpoint specifications
HC × Post	−0.0090 (0.277)	−0.0099 (0.245)	−0.0116 (0.232)	−0.0122 (0.272)	−0.0132 (0.252)	No statistically significant regime-dependent shift

Notes: The baseline breakpoint is 2011, corresponding to the beginning of China's Twelfth Five-Year Plan period. Alternative breakpoint years include 2010, 2012, 2013, and 2014. The table reports the interaction coefficient between each driver and the post-break indicator, with *p*-values in parentheses. The same stability-selected driver set is used across all specifications to ensure comparability. Significance levels: ** $p < 0.05$, *** $p < 0.01$.

Appendix D. Robustness Checks Using Local-Neighborhood and Inverse-Distance Spatial Weights Matrices

This appendix reports robustness checks for the GTWR residual spatial autocorrelation diagnostics under alternative spatial weights matrices. The baseline matrix is a row-standardized k = 3 nearest-neighbor matrix, which represents local-neighborhood proximity within the 11-city Guanzhong Plain Urban Agglomeration. To assess whether the residual diagnostics are sensitive to the definition of local-neighborhood structure, two additional k-nearest-neighbor matrices, k = 4 and k = 5, are used. An inverse-distance matrix based on inter-city geographic distance is also included to represent a distance-decay spatial relationship. All spatial weights matrices are constructed at the city level and applied year by year.

The results show that GTWR residuals do not exhibit statistically significant year-specific global spatial autocorrelation under any of the tested spatial weights matrices (Table A11). Under the baseline k = 3 specification, the mean Moran's I across 2000–2023 is −0.303, with a mean *p*-value of 0.819, and no year is significant at the 5% level. The robustness specifications yield similar conclusions: the mean Moran's I values are −0.175 for k = 4, −0.150 for k = 5, and −0.122 for the inverse-distance matrix, and none of these specifications produces significant year-specific residual spatial autocorrelation at the 5% level.

These results indicate that the GTWR residual spatial diagnostics are robust across the tested local-neighborhood and geographic distance spatial weights specifications. They also suggest that the GTWR model has adequately captured the main spatiotemporal structure of UER under the spatial relationship assumptions considered in this study. Because the robustness checks are limited to k-nearest-neighbor and inverse-distance matrices, the spatial-lag results are interpreted cautiously as supplementary diagnostic evidence rather than as conclusive evidence of stable spatial spillover effects under all possible spatial weights definitions.

Table A11. Sensitivity of GTWR residual Moran's I to alternative spatial weights matrices.

Spatial Weights Matrix	Role	Mean Moran's I	SD	Min Moran's I	Max Moran's I	Mean *p*-Value	Share Significant at 5%	Interpretation
k = 3 nearest neighbors	Baseline	−0.303	0.124	−0.508	−0.133	0.819	0.000	No significant residual spatial autocorrelation
k = 4 nearest neighbors	Robustness	−0.175	0.070	−0.308	−0.014	0.691	0.000	Robust
k = 5 nearest neighbors	Robustness	−0.150	0.039	−0.230	−0.085	0.664	0.000	Robust
Inverse-distance matrix	Robustness	−0.122	0.032	−0.175	−0.064	0.629	0.000	Robust

Notes: Moran's I statistics are calculated annually using GTWR residuals and then summarized across 2000–2023. "Share significant at 5%" denotes the proportion of years in which residual Moran's I is statistically significant at the 5% level.

Appendix E. Stability-Selection Threshold Sensitivity

To examine whether the robust driver set is sensitive to the stability-selection threshold, we recalculated the retained variable sets using more stringent selection-frequency cut-offs. The baseline threshold is $(\boldsymbol{\pi} \geq \mathbf{0.60})$, while alternative thresholds include $(\boldsymbol{\pi} \geq \mathbf{0.65})$, $(\boldsymbol{\pi} \geq \mathbf{0.70})$, $(\boldsymbol{\pi} \geq \mathbf{0.75})$, and $(\boldsymbol{\pi} \geq \mathbf{0.80})$. This sensitivity analysis evaluates whether the retained drivers form a stable and interpretable nested structure rather than being determined by a single arbitrary cut-off.

Table A12. Sensitivity of retained drivers to alternative stability-selection thresholds.

Threshold	Number of Retained Drivers	Retained Drivers	Interpretation
$(\pi \geq 0.60)$	10	TEC, HC, GDPG, TO, FI, TER, POP, HCI, MHL, URB	Baseline robust driver set
$(\pi \geq 0.65)$	10	TEC, HC, GDPG, TO, FI, TER, POP, HCI, MHL, URB	Same as baseline
$(\pi \geq 0.70)$	9	TEC, HC, GDPG, TO, FI, TER, POP, HCI, MHL	URB excluded
$(\pi \geq 0.75)$	9	TEC, HC, GDPG, TO, FI, TER, POP, HCI, MHL	Same as $(\pi \geq 0.70)$ if MHL is retained at $(\pi = 0.750)$
$(\pi \geq 0.80)$	7	TEC, HC, GDPG, TO, FI, TER, POP	More conservative core set

Notes: Selection frequency $(\boldsymbol{\pi})$ denotes the proportion of repeated subsampling runs in which a driver is selected with a non-zero Elastic Net coefficient. The baseline threshold $(\boldsymbol{\pi} \geq \mathbf{0.60})$ retains a parsimonious but inclusive driver set. More stringent thresholds produce nested subsets. TEC, HC, and FI remain stable across all tested thresholds, while MHL remains retained under thresholds up to $(\boldsymbol{\pi} \geq \mathbf{0.75})$ and is further supported by its clear period heterogeneity signal.

References

1. Seto, K.C.; Güneralp, B.; Hutyra, L.R. Global forecasts of urban expansion to 2030 and direct impacts on biodiversity and carbon pools. *Proc. Natl. Acad. Sci. USA* **2012**, *109*, 16083–16088. [CrossRef] [PubMed]
2. UN-Habitat. *World Cities Report 2020: The Value of Sustainable Urbanization*; United Nations Human Settlements Programme: Nairobi, Kenya, 2020.
3. Meerow, S.; Newell, J.P.; Stults, M. Defining urban resilience: A review. *Landsc. Urban Plan.* **2016**, *147*, 38–49. [CrossRef]
4. Bai, X.; Shi, P.; Liu, Y. Realizing China's urban dream. *Nature* **2014**, *509*, 158–160. [CrossRef] [PubMed]

5. National Development and Reform Commission (NDRC). *Outline of the Twelfth Five-Year Plan for National Economic and Social Development of the People's Republic of China (2011–2015)*; NDRC: Beijing, China, 2011.
6. Wang, H.; Wang, Y.; Ding, X.; Tang, J.; Li, R.; Li, K. Spatio-temporal evolution and driving mechanisms of ecological resilience: The Guanzhong Plain Urban Agglomeration case. *Environ. Sustain. Indic.* **2026**, *30*, 101229. [CrossRef]
7. York, R.; Rosa, E.A.; Dietz, T. STIRPAT, IPAT and ImPACT: Analytic tools for unpacking the driving forces of environmental impacts. *Ecol. Econ.* **2003**, *46*, 351–365. [CrossRef]
8. Liddle, B. What are the carbon emissions elasticities for income and population? Bridging STIRPAT and EKC via robust heterogeneous panel estimates. *Glob. Environ. Change* **2015**, *31*, 62–73. [CrossRef]
9. Shuai, C.; Chen, X.; Wu, Y.; Tan, Y.; Zhang, Y.; Shen, L. Identifying the key impact factors of carbon emission in China: Results from a largely expanded pool of potential impact factors. *J. Clean. Prod.* **2018**, *175*, 612–623. [CrossRef]
10. Tibshirani, R. Regression shrinkage and selection via the lasso. *J. R. Stat. Soc. Ser. B (Methodol.)* **1996**, *58*, 267–288. [CrossRef]
11. Brunsdon, C.; Fotheringham, A.S.; Charlton, M. Geographically weighted regression: A method for exploring spatial nonstationarity. *Geogr. Anal.* **1996**, *28*, 281–298. [CrossRef]
12. Huang, B.; Wu, B.; Barry, M. Geographically and temporally weighted regression for modeling spatio-temporal variation in house prices. *Int. J. Geogr. Inf. Sci.* **2010**, *24*, 383–401. [CrossRef]
13. Zou, H.; Hastie, T. Regularization and variable selection via the elastic net. *J. R. Stat. Soc. Ser. B (Stat. Methodol.)* **2005**, *67*, 301–320. [CrossRef]
14. Walker, B.; Holling, C.S.; Carpenter, S.R.; Kinzig, A. Resilience, adaptability and transformability in social–ecological systems. *Ecol. Soc.* **2004**, *9*, 5. [CrossRef]
15. Folke, C. Resilience: The emergence of a perspective for social–ecological systems analyses. *Glob. Environ. Change* **2006**, *16*, 253–267. [CrossRef]
16. Pickett, S.T.A.; Cadenasso, M.L.; McGrath, B. (Eds.) *Resilience in Ecology and Urban Design: Linking Theory and Practice for Sustainable Cities*; Springer: Dordrecht, The Netherlands, 2013. [CrossRef]
17. Meinshausen, N.; Bühlmann, P. Stability selection. *J. R. Stat. Soc. Ser. B (Stat. Methodol.)* **2010**, *72*, 417–473. [CrossRef]
18. Anselin, L. *Spatial Econometrics: Methods and Models*; Kluwer Academic Publishers: Dordrecht, The Netherlands, 1988. [CrossRef]
19. LeSage, J.P.; Pace, R.K. *Introduction to Spatial Econometrics*; CRC Press: Boca Raton, FL, USA, 2009. [CrossRef]
20. Wooldridge, J.M. *Econometric Analysis of Cross Section and Panel Data*, 2nd ed.; MIT Press: Cambridge, MA, USA, 2010.
21. Fu, B.; Wang, Y.; Lü, Y.; He, C.; Chen, L.; Song, C. The effects of land-use changes on the Loess Plateau of China. *Catena* **2007**, *72*, 13–26. [CrossRef]
22. National Development and Reform Commission (NDRC). *Development Plan for the Guanzhong Plain Urban Agglomeration*; NDRC: Beijing, China, 2018.
23. State Council of China. *Outline of the Plan for Ecological Protection and High-Quality Development of the Yellow River Basin*; State Council: Beijing, China, 2021.
24. National Bureau of Statistics of China (NBS). *China Statistical Yearbook*; China Statistics Press: Beijing, China, 2021.
25. Zhao, C.X.; Liu, Y.L.; Yan, Z.X.; Xi, J.L. Coupled coordination relationships between economy and ecosystem services at the county scale: Evidence from the Guanzhong Plain urban agglomeration in China. *J. Urban Plan. Dev.* **2025**, *151*, 04025045. [CrossRef]
26. Yang, J.; Huang, X. The 30 m annual land cover dataset and its dynamics in China from 1990 to 2019. *Earth Syst. Sci. Data* **2021**, *13*, 3907–3925. [CrossRef]
27. Liu, J.; Kuang, W.; Zhang, Z.; Xu, X.; Qin, Y.; Ning, J.; Zhou, W.; Zhang, S.; Li, R.; Yan, C.; et al. Spatiotemporal characteristics, patterns, and causes of land-use changes in China since the late 1980s. *J. Geogr. Sci.* **2014**, *24*, 195–210. [CrossRef]
28. National Bureau of Statistics of China (NBS). *China Statistical Yearbook*; China Statistics Press: Beijing, China, 2023.
29. IPCC. *2006 IPCC Guidelines for National Greenhouse Gas Inventories*; Institute for Global Environmental Strategies: Hayama, Japan, 2006.
30. Wu, J.; Niu, Y.; Peng, J.; Huang, X. Dynamics of energy consumption in prefecture-level cities of China from 1995 to 2009 based on DMSP/OLS nighttime light data. *Geogr. Res.* **2014**, *33*, 625–634. [CrossRef]
31. Mi, Z.; Liu, J.; Guan, D.; Su, B.; Liu, Z.; Wei, W.; Davis, S.J.; Coffman, D.M. Consumption-based emission accounting for Chinese cities. *Resour. Conserv. Recycl.* **2017**, *116*, 121–129. [CrossRef]
32. Little, R.J.A.; Rubin, D.B. *Statistical Analysis with Missing Data*, 3rd ed.; Wiley: Hoboken, NJ, USA, 2019.
33. Holling, C.S. Resilience and stability of ecological systems. *Annu. Rev. Ecol. Syst.* **1973**, *4*, 1–23. [CrossRef]
34. Cutter, S.L.; Burton, C.G.; Emrich, C.T. Disaster resilience indicators for benchmarking baseline conditions. *J. Homel. Secur. Emerg. Manag.* **2008**, *5*, 1–22. [CrossRef]
35. Wang, Y.; Cai, Y.; Xie, Y.; Zhang, P.; Chen, L. A quantitative framework to evaluate urban ecological resilience: Broadening understanding through multi-attribute perspectives. *Front. Ecol. Evol.* **2023**, *11*, 1144244. [CrossRef]

36. Costanza, R.; d'Arge, R.; de Groot, R.; Farber, S.; Grasso, M.; Hannon, B.; Limburg, K.; Naeem, S.; O'Neill, R.V.; Paruelo, J.; et al. The value of the world's ecosystem services and natural capital. *Nature* **1997**, *387*, 253–260. [CrossRef]
37. Xie, G.D.; Zhen, L.; Lu, C.X.; Xiao, Y.; Chen, C. Expert knowledge-based valuation method of ecosystem services in China. *J. Nat. Resour.* **2008**, *23*, 913–919. [CrossRef]
38. Xie, G.; Zhang, C.; Zhang, L.; Chen, W.; Li, S. Improvement of the ecosystem service valuation method based on unit area value equivalent factor. *J. Nat. Resour.* **2015**, *30*, 1243–1254. [CrossRef]
39. McGarigal, K.; Cushman, S.A.; Ene, E. *FRAGSTATS v4: Spatial Pattern Analysis Program for Categorical Maps*; University of Massachusetts: Amherst, MA, USA, 2012.
40. Shannon, C.E. A mathematical theory of communication. *Bell Syst. Tech. J.* **1948**, *27*, 379–423. [CrossRef]
41. With, K.A. Using fractal analysis to assess how species perceive landscape structure. *Landsc. Ecol.* **1994**, *9*, 25–36. [CrossRef]
42. Hargis, C.D.; Bissonette, J.A.; David, J.L. The behavior of landscape metrics commonly used in the study of habitat fragmentation. *Landsc. Ecol.* **1998**, *13*, 167–186. [CrossRef]
43. Peng, J.; Liu, Y.; Li, T.; Wu, J. Regional ecosystem health response to rural land use change: A case study in Lijiang City. *Ecol. Indic.* **2015**, *72*, 399–410. [CrossRef]
44. Meng, Z.; He, M.; Li, X.; Li, H.; Tan, Y.; Li, Z.; Wei, Y. Spatio-temporal analysis and driving forces of urban ecosystem resilience based on land use: A case study in the Great Bay Area. *Ecol. Indic.* **2024**, *159*, 111769. [CrossRef]
45. Xia, C.Y.; Dong, Z.Y.Z.; Chen, B. Spatio-temporal analysis and simulation of urban ecological resilience: A case study of Hangzhou. *Acta Ecol. Sin.* **2022**, *42*, 116–126. [CrossRef]
46. Xue, F.; Zhang, N.C.; Xia, C.Y.; Zhang, J.; Wang, C.Y.; Li, S.; Zhou, J. Spatial evaluation of urban ecological resilience and analysis of driving forces: A case study of Tongzhou District, Beijing. *Acta Ecol. Sin.* **2023**, *43*, 6810–6823.
47. Kan, D.; Lv, L. The impact of new urbanization on water ecological resilience: An empirical study from central China. *PLoS ONE* **2024**, *19*, e0313865. [CrossRef] [PubMed]
48. Dietz, T.; Rosa, E.A. Rethinking the environmental impacts of population, affluence and technology. *Hum. Ecol. Rev.* **1994**, *1*, 277–300.
49. Cameron, A.C.; Miller, D.L. A practitioner's guide to cluster-robust inference. *J. Hum. Resour.* **2015**, *50*, 317–372. [CrossRef]
50. Belloni, A.; Chernozhukov, V.; Hansen, C. Inference on treatment effects after selection among high-dimensional controls. *Rev. Econ. Stud.* **2014**, *81*, 608–650. [CrossRef]
51. Chernozhukov, V.; Hansen, C.; Spindler, M. Post-selection and post-regularization inference in linear models with many controls. *Am. Econ. Rev.* **2015**, *105*, 486–490. [CrossRef]
52. Friedman, J.; Hastie, T.; Tibshirani, R. Regularization Paths for Generalized Linear Models via Coordinate Descent. *J. Stat. Softw.* **2010**, *33*, 1–22. [CrossRef]
53. Fotheringham, A.S.; Brunsdon, C.; Charlton, M. *Geographically Weighted Regression: The Analysis of Spatially Varying Relationships*; Wiley: Chichester, UK, 2002.
54. Hurvich, C.M.; Simonoff, J.S.; Tsai, C.-L. Smoothing parameter selection in nonparametric regression using an improved Akaike information criterion. *J. R. Stat. Soc. Ser. B (Stat. Methodol.)* **1998**, *60*, 271–293. [CrossRef]
55. Hyndman, R.J.; Koehler, A.B. Another look at measures of forecast accuracy. *Int. J. Forecast.* **2006**, *22*, 679–688. [CrossRef]
56. Shapiro, S.S.; Wilk, M.B. An analysis of variance test for normality (complete samples). *Biometrika* **1965**, *52*, 591–611. [CrossRef]
57. Moran, P.A.P. Notes on continuous stochastic phenomena. *Biometrika* **1950**, *37*, 17–23. [CrossRef]
58. Meerow, S.; Newell, J.P. Urban resilience for whom, what, when, where, and why? *Urban Geogr.* **2019**, *40*, 309–329. [CrossRef]
59. Davoudi, S. Resilience: A bridging concept or a dead end? *Plan. Theory Pract.* **2012**, *13*, 299–307. [CrossRef]
60. Tozer, L.; Bulkeley, H.; Kiss, B.; Luque-Ayala, A.; Palgan, Y.V.; McCormick, K.; Wamsler, C. Nature for resilience? The politics of governing urban nature. *Ann. Am. Assoc. Geogr.* **2023**, *113*, 599–615. [CrossRef]
61. Liang, L.; Liu, X.; Ge, P. The fairness evaluation on achieving Sustainable Development Goals (SDGs) of ecological footprint: A case study of the Guanzhong Plain urban agglomeration. *Sustainability* **2025**, *17*, 4728. [CrossRef]
62. Chen, J.; Wang, S.; Zou, Y. Construction of an ecological security pattern based on ecosystem sensitivity and the importance of ecological services: A case study of the Guanzhong Plain urban agglomeration, China. *Ecol. Indic.* **2022**, *136*, 108688. [CrossRef]
63. Chelleri, L.; Waters, J.J.; Olazabal, M.; Minucci, G. Resilience trade-offs: Addressing multiple scales and temporal aspects of urban resilience. *Environ. Urban.* **2015**, *27*, 181–198. [CrossRef]
64. Chang, Q.; Yang, R.; Zhong, Y.; Sun, L. The coupling coordination and driving factors of urbanization and ecological resilience in the Yangtze River Delta urban agglomeration, China. *Land* **2024**, *13*, 111. [CrossRef]
65. Lowe, M.; Bell, S.; Briggs, J.; McMillan, E.; Morley, M.; Grenfell, M.; Sweeting, D.; Whitten, A.; Jordan, N. A research-based, practice-relevant urban resilience framework for local government. *Local Environ.* **2024**, *29*, 886–901. [CrossRef]
66. Angheloiu, C.; Tennant, M. Mind the gap: Defining urban resilience knowledge-implementation gaps. *J. City Clim. Policy Econ.* **2024**, *2*, 316–358. [CrossRef]

67. Ye, H.; Song, Y.; Xue, D.; Xia, S.; Tang, Y.; Zhang, L. Construction of an ecological security pattern for the Guanzhong Plain urban agglomeration: Scale perspective and hierarchy demand. *Front. Environ. Sci.* **2023**, *11*, 1136630. [CrossRef]
68. Meng, B.; Zhang, J.; Zhang, X. Detecting the spatial network structure of the Guanzhong Plain urban agglomeration, China: A multi-dimensional element flow perspective. *Land* **2023**, *12*, 563. [CrossRef]